LETTER

doi:10.1038/nature13706

RIPK1 ensures intestinal homeostasis by protecting the epithelium against apoptosis

Nozomi Takahashi[1,2], Lars Vereecke[1,2], Mathieu J. M. Bertrand[1,2], Linde Duprez[1,2], Scott B. Berger[3], Tatyana Divert[1,2], Amanda Gonçalves[1,2,4], Mozes Sze[1,2], Barbara Gilbert[1,2], Stephanie Kourula[1,2], Vera Goossens[1,2], Sylvie Lefebvre[1,2], Claudia Günther[5], Christoph Becker[5], John Bertin[3], Peter J. Gough[3], Wim Declercq[1,2], Geert van Loo[1,2] & Peter Vandenabeele[1,2,6]

Receptor interacting protein kinase 1 (RIPK1) has an essential role in the signalling triggered by death receptors and pattern recognition receptors[1,2]. RIPK1 is believed to function as a node driving NF-κB-mediated cell survival and inflammation as well as caspase-8 (CASP8)-dependent apoptotic or RIPK3/MLKL-dependent necroptotic cell death. The physiological relevance of this dual function has remained elusive because of the perinatal death of RIPK1 full knockout mice[3]. To circumvent this problem, we generated RIPK1 conditional knockout mice, and show that mice lacking RIPK1 in intestinal epithelial cells (IECs) spontaneously develop severe intestinal inflammation associated with IEC apoptosis leading to early death. This early lethality was rescued by antibiotic treatment, MYD88 deficiency or tumour-necrosis factor (TNF) receptor 1 deficiency, demonstrating the importance of commensal bacteria and TNF in the IEC *Ripk1* knockout phenotype. CASP8 deficiency, but not RIPK3 deficiency, rescued the inflammatory phenotype completely, indicating the indispensable role of RIPK1 in suppressing CASP8-dependent apoptosis but not RIPK3-dependent necroptosis in the intestine. RIPK1 kinase-dead knock-in mice did not exhibit any sign of inflammation, suggesting that RIPK1-mediated protection resides in its kinase-independent platform function. Depletion of RIPK1 in intestinal organoid cultures sensitized them to TNF-induced apoptosis, confirming the *in vivo* observations. Unexpectedly, TNF-mediated NF-κB activation remained intact in these organoids. Our results demonstrate that RIPK1 is essential for survival of IECs, ensuring epithelial homeostasis by protecting the epithelium from CASP8-mediated IEC apoptosis independently of its kinase activity and NF-κB activation.

RIPK1 is a serine/threonine kinase that is an upstream regulator of the cellular responses initiated by members of the death receptor families, such as TNF receptor (TNFR), and pattern recognition receptor superfamilies[1,2]. Downstream of TNFR1 (also known as TNFRSF1A), RIPK1 regulates two opposed cellular fates: cell survival via NF-κB-mediated gene induction, and cell death by induction of apoptosis or necroptosis. The kinase activity of RIPK1 is dispensable for its pro-survival function but essential for its killing potential[4,5]. When CASP8 is absent or inhibited, RIPK1 triggers TNF-mediated necroptosis through a phosphorylation-driven cascade involving RIPK3 as a partner[6–8] and MLKL as the downstream cell death executor[9,10]. When inhibitor of apoptosis (IAP), transforming-growth-factor-β-activated kinase 1 or NF-κB essential modulator are inhibited, RIPK1 mediates CASP8-dependent apoptosis[11–14]. The mechanisms by which RIPK1 switches from a pro-survival to a pro-death molecule are poorly understood but probably depend on its ubiquitination state[14–16]. The *in vivo* role of RIPK1 has been difficult to assess due to the perinatal mortality of full knockout mice[3]. Therefore, we generated a RIPK1 conditional knockout mouse line ($Ripk1^{fl/fl}$) by *loxP* technology (Extended Data Fig. 1a–c). $Ripk1^{-/-}$ progeny of $Ripk1^{fl/fl}$ mice crossed with Cre-deleter mice died soon after birth, as reported[3]. *Ripk1* depletion was confirmed in primary mouse embryonic fibroblasts (MEFs) (Extended Data Fig. 1d). Upon TNF stimulation, $Ripk1^{-/-}$ MEFs showed defective activation of mitogen-activated protein kinases (MAPKs) and canonical NF-κB associated with apoptosis (Extended Data Fig. 2a, b).

Defects in the NF-κB pathway resulting from deletion of NF-κB essential modulator or transforming-growth-factor-β-activated kinase 1 in IECs cause massive apoptosis and gut inflammation resembling inflammatory bowel disease[17,18]. However, RIPK3-dependent necroptosis was recently demonstrated to drive inflammatory-bowel-disease-like gut inflammation in mice with CASP8 or Fas-associated protein with death domain (FADD) deletion in IECs, identifying CASP8 and FADD as physiological suppressors of necroptosis[19,20]. Since RIPK1 has a role in both NF-κB activation and RIPK3-dependent cell death, we investigated the consequences of its deletion in IECs by crossing $Ripk1^{fl/fl}$ mice with villin-Cre transgenic mice to give an IEC-specific *Ripk1* knockout ($Ripk1^{IEC\text{-}KO}$). The progeny were born at a normal Mendelian ratio, but their growth was severely retarded and about 70% of them died within 4 weeks (Fig. 1a, b and Extended Data Fig. 3a). DNA and protein analysis of various organs from the $Ripk1^{IEC\text{-}KO}$ mice confirmed specific *Ripk1* deletion in the colon and small intestine (Extended Data Fig. 3b, c). The colon of $Ripk1^{IEC\text{-}KO}$ mice displays progressive inflammation characterized by the presence of inflammatory infiltrates, aberrant crypts, and loss of goblet cells and tissue architecture (Fig. 1c and Extended Data Fig. 3d) accompanied by apoptosis, as shown by terminal deoxynucleotidyl transferase dUTP nick end labelling (TUNEL) and CASP3 activation (Fig. 1c and Extended Data Fig. 3e). When *Ripk1* was deleted in adult $Ripk1^{fl/fl}$ *villin-cre-ERT2* transgenic mice (an inducible IEC knockout, $Ripk1^{iIEC\text{-}KO}$) by using 4-hydroxytamoxifen (4-OHT), massive intestinal cell death occurred and all the mice died. Thus, the phenotype of $Ripk1^{IEC\text{-}KO}$ mice is not neonate specific (Fig. 1d, e). Surviving $Ripk1^{IEC\text{-}KO}$ mice showed splenomegaly and colon shortening (Extended Data Fig. 4a), and colonoscopic analysis revealed lesions associated with inflammatory dysplasia (Fig. 1f), consistent with the histopathological findings (Extended Data Fig. 4b). The inflammation in the small intestine was also associated with a loss of tissue architecture and of mucus-producing goblet cells and antimicrobial peptide (AMP)-producing Paneth cells (Fig. 1g), resulting in physical barrier dysfunction and intestinal leakage, as shown by increased fluorescence in the serum of $Ripk1^{IEC\text{-}KO}$ mice fed with FITC-labelled dextran (Fig. 1h). Accordingly, expression of the AMPs lysozyme P and cryptidin 1 was decreased, whereas TNF production was increased (Fig. 1i). As cell death, inflammation and mortality were associated with bacterial colonization shortly after birth, we hypothesized that deletion of RIPK1 sensitized IECs to TNF that is produced upon sensing of commensal bacteria. This would result in barrier disruption, commensal infiltration and severe gut inflammation,

[1]VIB Inflammation Research Center, Technologiepark 927, B-9052 Ghent, Belgium. [2]Department of Biomedical Molecular Biology, Ghent University, Technologiepark 927, B-9052 Ghent, Belgium. [3]Pattern Recognition Receptor Discovery Performance Unit, Immuno-inflammation Therapeutic Area, GlaxoSmithKline, Collegeville, Pennsylvania 19426, USA. [4]VIB Bio Imaging Core Gent, Technologiepark 927, B-9052 Ghent, Belgium. [5]Department of Medicine 1, Friedrich-Alexander-University, D-91054 Erlangen, Germany. [6]Methusalem program, Ghent University, Technologiepark 927, B-9052 Ghent, Belgium.

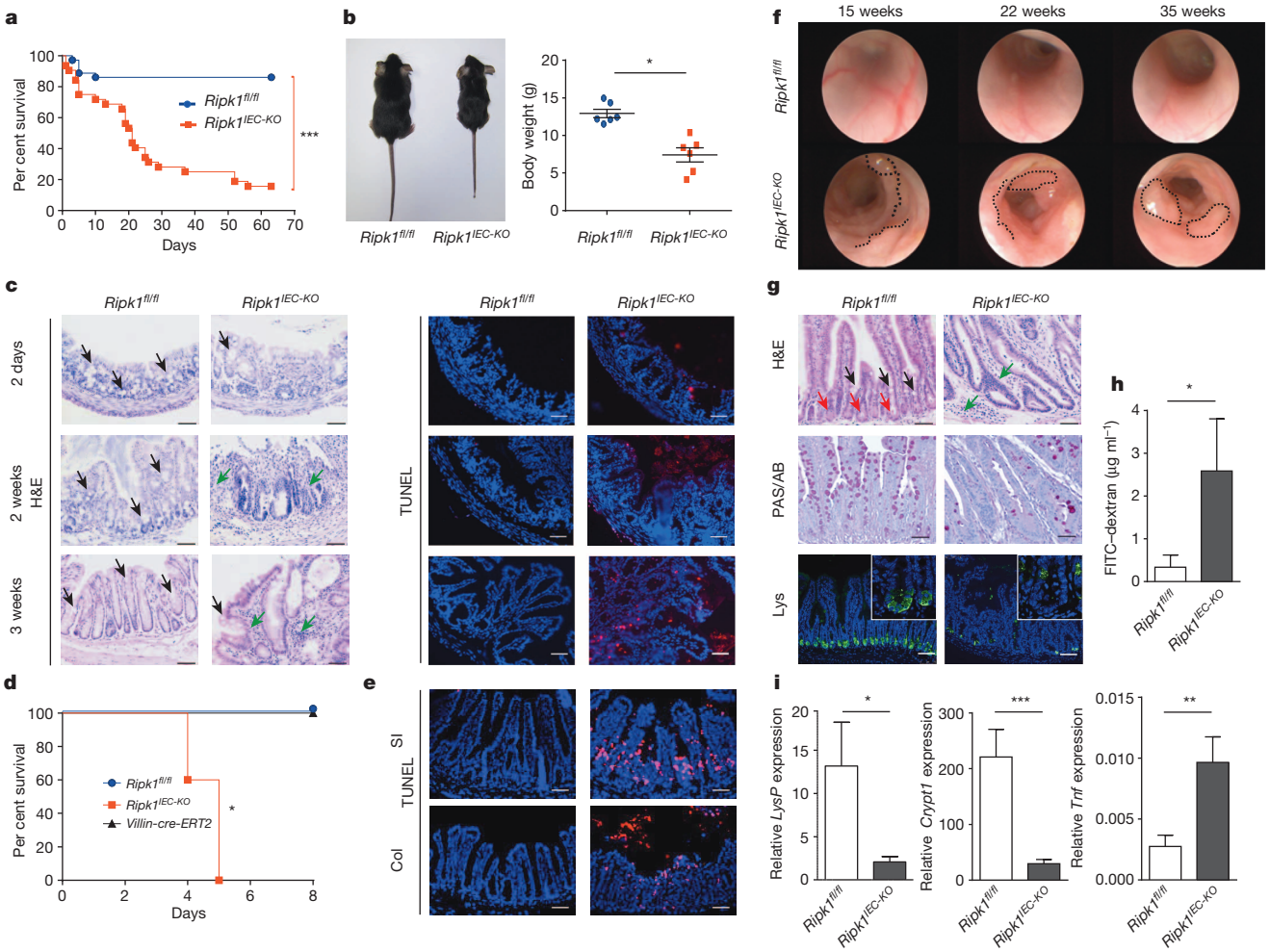

Figure 1 | Death and spontaneous gut inflammation in mice with RIPK1 deletion in IECs. **a**, Cumulative survival rate of *Ripk1*$^{IEC\text{-}KO}$ mice ($n = 34$) compared to *Ripk1*$^{fl/fl}$ mice ($n = 39$), ***$P < 0.0001$. **b**, Macroscopic features and body weight of *Ripk1*$^{IEC\text{-}KO}$ (3 weeks, $n = 6$) and sex-matched littermate *Ripk1*$^{fl/fl}$ mice ($n = 6$). *$P < 0.05$. Data represent mean ± standard error of the mean (s.e.m.). **c**, Haematoxylin and eosin staining (H&E; left panels) and TUNEL assay (red; right panels) of colon sections from *Ripk1*$^{fl/fl}$ and *Ripk1*$^{IEC\text{-}KO}$ mice. Black arrows, goblet cells; green arrows, infiltrating leukocytes (scale bars, 50 μm). **d**, Survival rates of *Ripk1*$^{fl/fl}$ ($n = 3$), *Ripk1*$^{fl/fl}$ *villin-cre-ERT2*^{Tg} (*Ripk1*$^{iIEC\text{-}KO}$) ($n = 5$) and *villin-cre-ERT2*^{Tg} mice ($n = 2$) treated with 1 mg 4-OHT daily; *$P < 0.05$. **e**, TUNEL assay (red) in small intestine (SI) and colon (Col) of *Ripk1*$^{fl/fl}$ and *Ripk1*$^{iIEC\text{-}KO}$ mice after three daily 4-OHT injections (scale bars, 25 μm). Representative images of *Ripk1*$^{fl/fl}$ ($n = 3$) and *Ripk1*$^{IEC\text{-}KO}$ ($n = 3$) mice. **f**, Endoscopic images of *Ripk1*$^{IEC\text{-}KO}$ and littermate *Ripk1*$^{fl/fl}$ mice. Dotted lines show irregular surface and lesions. **g**, Haematoxylin and eosin and periodic acid–Schiff/Alcian blue (PAS/AB; goblet cells) staining and lysozyme (Lys) (Paneth cells) immunohistochemical staining in the small intestine. Black arrows, goblet cells; red arrows, Paneth cells; green arrows, infiltrating leukocytes (scale bars, 50 μm). **h**, Intestinal permeability assay in *Ripk1*$^{IEC\text{-}KO}$ ($n = 3$) and *Ripk1*$^{fl/fl}$ mice ($n = 3$) using FITC-labelled dextran. Data represent mean ± s.e.m. *$P < 0.05$. **i**, Quantitative real-time PCR (qPCR) analysis of antimicrobial peptides and TNF on RNA extracted from small intestine mucosa of *Ripk1*$^{IEC\text{-}KO}$ ($n = 8$) and control *Ripk1*$^{fl/fl}$ mice ($n = 8$). *$P < 0.05$, **$P < 0.01$, ***$P < 0.001$. Data represent mean ± s.e.m. LysP, lysozyme P; Crypt1, cryptidin 1.

exacerbate TNF production and lead to the death of *Ripk1*$^{IEC\text{-}KO}$ mice. We tested our hypothesis by using a cocktail of broad-spectrum antibiotics and by a genetic approach using mice deficient in MYD88—an essential adaptor protein in the signalling pathways activated downstream of toll-like receptors (TLRs) in response to pathogen-associated molecular pattern sensing—or mice deficient in TNFR1. Antibiotic treatment starting in the mother 2 weeks before birth of the offspring significantly improved the viability of *Ripk1*$^{IEC\text{-}KO}$ mice and reduced inflammation and apoptosis in the majority of mice (Fig. 2a, b and Extended Data Fig. 5a, b). Body size, spleen size, colon length (Fig. 2c), number of Paneth cells (Extended Data Fig. 5b) and TNF level (Extended Data Fig. 5c) were normalized. The use of antibiotics also significantly prolonged the survival of adult *Ripk1*$^{iIEC\text{-}KO}$ mice following 4-OHT-induced *Ripk1* deletion (Extended Data Fig. 5d). In agreement, MYD88 significantly delayed the death of *Ripk1*$^{IEC\text{-}KO}$ mice (Fig. 2d and Extended Data Fig. 6a). Nevertheless, histological signs of intestinal inflammation and apoptosis persisted in *Ripk1*$^{IEC\text{-}KO}$ *Myd88*$^{-/-}$ mice (Fig. 2e and Extended Data Fig. 6c), indicating the involvement of additional MYD88-independent pathways. TNFR1 deficiency also significantly protected *Ripk1*$^{IEC\text{-}KO}$ mice from death (Fig. 2f and Extended Data Fig. 6b), and although mild inflammation remained, apoptosis was inhibited in *Ripk1*$^{IEC\text{-}KO}$ *Tnfr1*$^{-/-}$ mice (Fig. 2g and Extended Data Fig. 6d). These observations indicate that bacterial colonization and subsequent production of TNF are crucial for amplification of apoptosis, contributing to intestinal inflammation and death.

We then examined whether blocking cell death in IECs would rescue the inflammatory phenotype by generating *Ripk1*$^{IEC\text{-}KO}$ *Casp8*$^{IEC\text{-}KO}$ and *Ripk1*$^{IEC\text{-}KO}$ *Ripk3*$^{-/-}$ double knockout mice. *Ripk1*$^{IEC\text{-}KO}$ *Casp8*$^{IEC\text{-}KO}$ mice were born at a normal Mendelian ratio, grew normally until adulthood and were macroscopically indistinguishable from *Ripk1*$^{fl/fl}$ *Casp8*$^{fl/fl}$ control mice (Fig. 3a and Extended Data Fig. 7a, b). In contrast *Ripk1*$^{IEC\text{-}KO}$ *Ripk3*$^{-/-}$ mice are phenotypically identical to *Ripk1*$^{IEC\text{-}KO}$ mice (Fig. 3b and Extended Data Fig. 7c, d), excluding a role for RIPK3-dependent necroptosis[6], inflammation[21] or apoptosis[13] in the *Ripk1*$^{IEC\text{-}KO}$

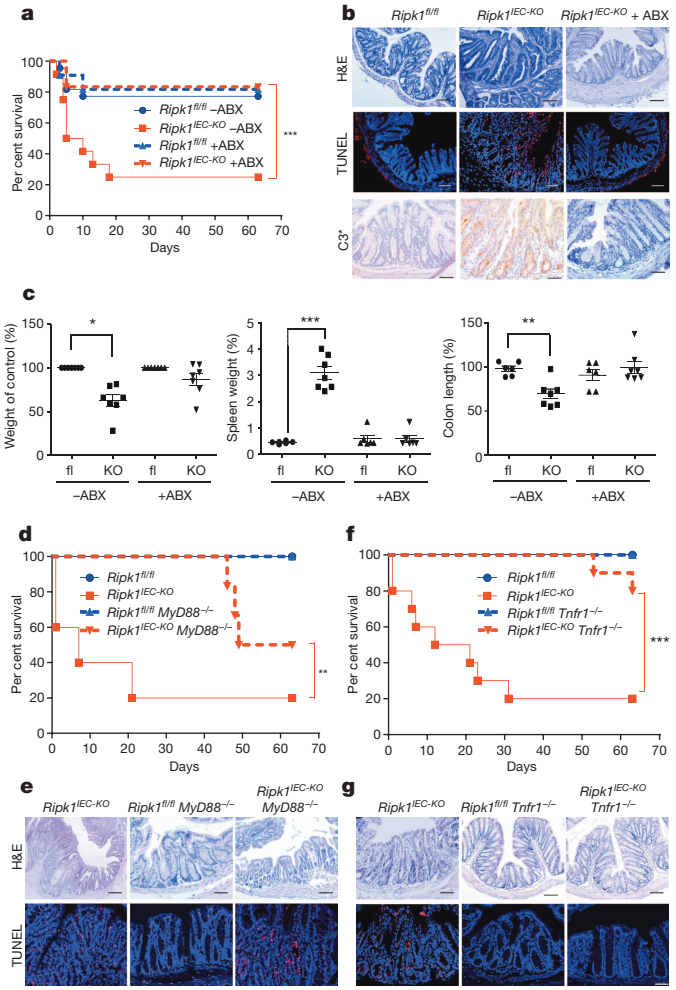

Figure 2 | *Ripk1*$^{IEC\text{-}KO}$ phenotype in conditions of antibiotic treatment, MYD88 deficiency, or TNFR1 deficiency. **a**, Breeding couples were treated with broad-spectrum antibiotics (+ABX) 2 weeks before the birth of offspring, and survival rates of *Ripk1*$^{fl/fl}$ ($n = 18$) and *Ripk1*$^{IEC\text{-}KO}$ mice ($n = 12$) were compared to untreated controls (−ABX). ***$P = 0.0008$. **b**, Haematoxylin and eosin staining and TUNEL assay (red) and active CASP3 (C3*) immunohistochemistry (brown) of *Ripk1*$^{IEC\text{-}KO}$ and *Ripk1*$^{fl/fl}$ mice treated as in **a**. Representative image of *Ripk1*$^{fl/fl}$ ($n = 3$), untreated *Ripk1*$^{IEC\text{-}KO}$ ($n = 7$) and antibiotic-treated *Ripk1*$^{IEC\text{-}KO}$ mice ($n = 7$). **c**, Body size ratio (expressed as percent relative to littermate), spleen weight and colon length of 6–12-week-old *Ripk1*$^{IEC\text{-}KO}$ ($n = 7$) and littermate *Ripk1*$^{fl/fl}$ mice ($n = 6$) with or without antibiotics. *$P < 0.05$, **$P < 0.005$, ***$P < 0.0001$. Data represent mean ± s.e.m. **d**, Survival rate of *Ripk1*$^{IEC\text{-}KO}$ *Myd88*$^{-/-}$ ($n = 5$) compared to *Ripk1*$^{IEC\text{-}KO}$ ($n = 5$), control *Ripk1*$^{fl/fl}$ ($n = 5$) and *Ripk1*$^{fl/fl}$ *Myd88*$^{-/-}$ mice ($n = 6$). **$P < 0.001$. **e**, Haematoxylin and eosin staining (scale bars, 100 μm) and TUNEL assay (scale bars, 25 μm) of colon sections from *Ripk1*$^{fl/fl}$ *Myd88*$^{-/-}$ and *Ripk1*$^{IEC\text{-}KO}$ *Myd88*$^{-/-}$ mice. **f**, Survival rate of *Ripk1*$^{IEC\text{-}KO}$ *Tnfr1*$^{-/-}$ ($n = 9$), *Ripk1*$^{IEC\text{-}KO}$ ($n = 10$), control *Ripk1*$^{fl/fl}$ ($n = 11$) and *Ripk1*$^{fl/fl}$ *Tnfr1*$^{-/-}$ mice ($n = 7$). ***$P < 0.0001$. **g**, Haematoxylin and eosin staining (scale bars, 100 μm) and TUNEL assay (scale bars, 25 μm) of colon sections from *Ripk1*$^{fl/fl}$ *Tnfr1*$^{-/-}$ and *Ripk1*$^{IEC\text{-}KO}$*Tnfr1*$^{-/-}$ mice.

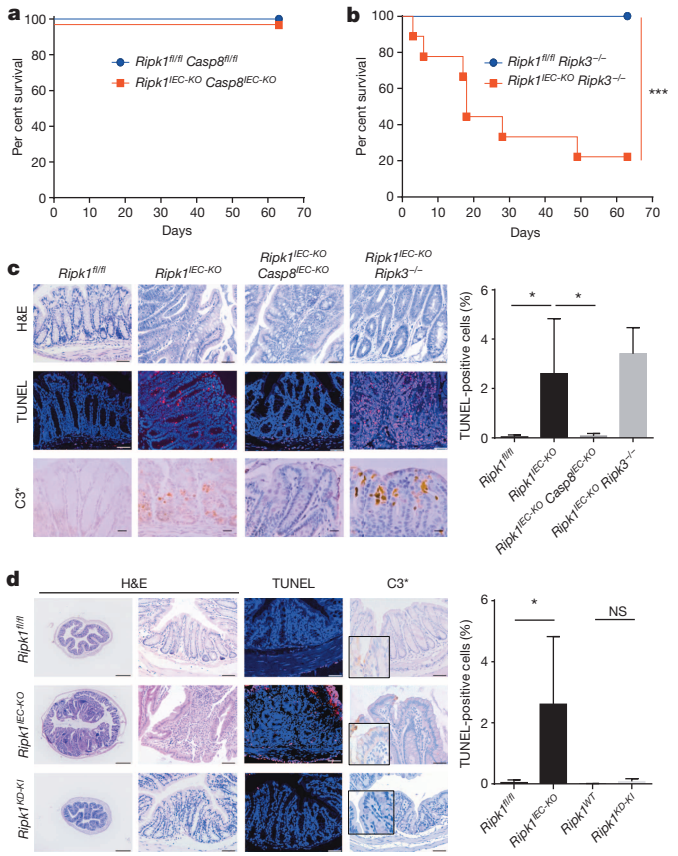

Figure 3 | Lethality of *Ripk1*$^{iIEC\text{-}KO}$ in mice requires *Casp8* but not RIPK3 or RIPK1 kinase activity. **a**, Survival rate of *Ripk1*$^{IEC\text{-}KO}$ *Casp8*$^{IEC\text{-}KO}$ mice ($n = 6$) and control *Ripk1*$^{fl/fl}$;*Casp8*$^{fl/fl}$ mice ($n = 8$). **b**, Survival rate of *Ripk1*$^{IEC\text{-}KO}$ *Ripk3*$^{-/-}$ mice ($n = 9$) and control *Ripk1*$^{fl/fl}$ *Ripk3*$^{-/-}$ mice ($n = 9$). ***$P < 0.0001$. **c**, Histopathological analysis of colons of *Ripk1*$^{fl/fl}$ ($n = 4$), *Ripk1*$^{IEC\text{-}KO}$ ($n = 4$), *Ripk1*$^{IEC\text{-}KO}$ *Casp8*$^{IEC\text{-}KO}$ ($n = 4$) and *Ripk1*$^{IEC\text{-}KO}$*Ripk3*$^{-/-}$ mice ($n = 3$) by haematoxylin and eosin staining and TUNEL assay (red; quantification in the right panel), and active CASP3 immunohistochemistry (C3*; brown). Scale bars, 50 μm. **d**, Histopathological analysis of colon samples from 12-week-old *Ripk1*$^{fl/fl}$ ($n = 3$), *Ripk1*$^{IEC\text{-}KO}$ ($n = 3$) and RIPK1-kinase-dead knock-in mice (*Ripk1*$^{KD\text{-}KI}$, $n = 5$) by haematoxylin and eosin staining and TUNEL assay (red; quantification in the right panel), and active CASP3 immunohistochemistry (C3*; brown). Scale bars, 50 μm. *$P < 0.05$. Data represent mean ± s.e.m. WT, wild type; NS, not significant.

phenotype. Histopathological analysis of the colons revealed complete protection from apoptosis and inflammation by concomitant deletion of *Casp8* but not of *Ripk3* (Fig. 3c). This demonstrates that *Ripk1*$^{IEC\text{-}KO}$ mice develop lethal inflammation due to excessive CASP8-dependent apoptosis of IECs, identifying RIPK1 as an apoptosis suppressor in the intestine. Complete rescue by deletion of CASP8 but not by TNFR1 deletion suggests that stimuli other than TNF might account for IEC apoptosis and inflammation and that other death-inducing stimuli converge at CASP8. However, the spontaneous ileitis caused by uncontrolled necroptosis in *Casp8*$^{IEC\text{-}KO}$ mice, as reported earlier[20], persisted in *Ripk1*$^{IEC\text{-}KO}$ *Casp8*$^{IEC\text{-}KO}$ mice, indicating that absence of RIPK1 does not protect *Casp8*$^{IEC\text{-}KO}$ mice against necroptosis in the ileum (Extended Data Fig. 7e, f).

Because RIPK1 mediates both kinase-dependent and -independent functions[1,2], we evaluated the requirement for its enzymatic activity by characterizing a RIPK1 kinase-dead knock-in mouse line (*Ripk1*$^{KD\text{-}KI}$)[4,5]. Unlike the *Ripk1*$^{-/-}$[17] and *Ripk1*$^{IEC\text{-}KO}$ mice, *Ripk1*$^{KD\text{-}KI}$ mice were viable and grew normally into adults[4,5]. The colon (Fig. 3d) and small intestine (Extended Data Fig. 8) of *Ripk1*$^{KD\text{-}KI}$ mice showed no sign of inflammation or apoptosis. This indicates that the *Ripk1*$^{IEC\text{-}KO}$ phenotype is caused by loss of the RIPK1 platform-mediated function, as the kinase activity of RIPK1 is totally dispensable for the maintenance of intestinal homeostasis.

To investigate the mechanism of apoptosis in IECs further, we established intestinal organoid cultures[22]. Because crypt cells from *Ripk1*$^{IEC\text{-}KO}$ mice failed to grow into organoids (data not shown), we depleted RIPK1 in organoids derived from *Ripk1*$^{iIEC\text{-}KO}$ mice by *in vitro* 4-OHT treatment. In accordance with our observations that death of IECs in *Ripk1*$^{IEC\text{-}KO}$ mice is associated with increased *Tnf* mRNA levels in intestinal tissue (Fig. 1i), and that absence of TNFR1 rescues perinatal

death (Fig. 2f, g), we found that TNF treatment induced massive apoptosis in the *Ripk1*-depleted organoids but not in the control ones (Fig. 4a and Supplementary Videos 1–4), demonstrating enhanced sensitivity towards TNF as compared to control. In agreement, CASP8 and CASP3 were activated only in lysates from *Ripk1*-depleted cultures (Fig. 4b). Reportedly, RIPK1 mediates TNF-dependent canonical NF-κB activation independently of its kinase activity, and the sensitivity of the RIPK1-deficient MEFs to TNF-mediated apoptosis has been explained, at least in part, by defective induction of NF-κB-dependent pro-survival genes[3] (Extended Data Fig. 2). Notably, the sensitization of *Ripk1*-depleted organoids to TNF-induced apoptosis was not associated with defects in canonical NF-κB activation. IκBα phosphorylation and degradation occurred with similar efficiency and kinetics in both cultures regardless of *Ripk1* depletion (Fig. 4b). Intact NF-κB activation was further confirmed by analysing the induction of NF-κB-dependent genes in the organoid culture. Expression of these target genes did not decrease, while *Ripk1* depletion by 4-OHT treatment exceeded 90% (Fig. 4c). Finally, we confirm *in vitro* that the sensitization of RIPK1-deficient IECs to apoptosis is independent of the kinase function (Fig. 3d), as organoids derived from $Ripk1^{KD\text{-}KI}$ mice were not sensitized to TNF (Fig. 4d–f and Supplementary Video 5). RIPK1-depleted organoids eventually died after 4 days without exogenous stimuli, confirming an essential role of RIPK1 for survival of IECs (Extended Data Fig. 9a and Supplementary Videos 6 and 7). Whether this TNF-independent cell death or additional death receptor ligands contribute to *in vivo* phenotype remains unknown, but administration of prototype pathogen-associated molecular patterns such as lipopolysaccharide and lipoteichoic acid do not directly induce cell death of intestinal organoids (Extended Data Fig. 9b, c).

In conclusion, we demonstrate that RIPK1 has a crucial kinase-independent role in protecting IECs from CASP8-dependent apoptosis by maintaining intestinal homeostasis. Low constitutive levels of TNF secreted in the mucosa may be sufficient to kill IECs lacking RIPK1 and partially disrupt the intestinal barrier, allowing commensal bacteria to infiltrate and activate innate immunity. The consequent increase in TNF fuels a cycle of IEC apoptosis and inflammation in mice lacking homeostatic control by RIPK1. Notably, RIPK1 deficiency sensitizes IECs to TNF-mediated apoptosis independently of any defect in NF-κB activation, whereas sensitization of RIPK1-deficient MEFs was associated with defective NF-κB, revealing an unexpected pro-survival role of RIPK1 downstream of TNF in IECs. Of note, one study suggested that RIPK1 protects MEFs from TNF-mediated CASP8-dependent apoptosis by promoting cFLIP stability independently of canonical NF-κB activation[23] (Extended Data Fig. 10a). We observed a modest decrease of cFLIP level in RIPK1-depleted IECs stimulated with TNF, but the biological relevance of this observation remains unclear (Extended Data Fig. 10b). This platform-dependent anti-apoptotic RIPK1 function might exist in several cell types, as RIPK1 depletion in L929 cells also sensitized them to TNF-induced CASP8-dependent apoptosis[24]. Our results support a novel concept that CASP8 keeps RIPK1 and RIPK3 necroptotic signalling in check[19,25,26], while RIPK1 protects cells from excessive CASP8 activation in response to mild triggering with death receptor ligands or cellular stress. This means that the RIPK1–CASP8 node is the crucial decision point in cell death or survival and explains why cells can switch so easily from apoptosis to necroptosis and vice versa, when either cell death pathway is blocked[24,27]. In contrast to three recent papers reporting that rescuing the lethality of RIPK1 full knockout requires simultaneous block of CASP8-dependent apoptosis and RIPK3-dependent necroptosis[28–30], we found that blocking apoptosis alone rescues intestinal inflammation. This finding indicates that the default cell death mode is tissue specific. Together, our results emphasize that RIPK1 is an essential survival factor in intestinal homeostasis. An accompanying paper[31] presents similar data. Notably, different approaches to rescue the phenotype of $Ripk1^{IEC\text{-}KO}$ mice by either ablating CASP8 (our study) or FADD (ref. 31) prevented IEC apoptosis caused by RIPK1 deficiency. However, necroptosis in IECs caused by deficiency of CASP8 or FADD cannot be prevented by loss of RIPK1, suggesting RIPK1-independent

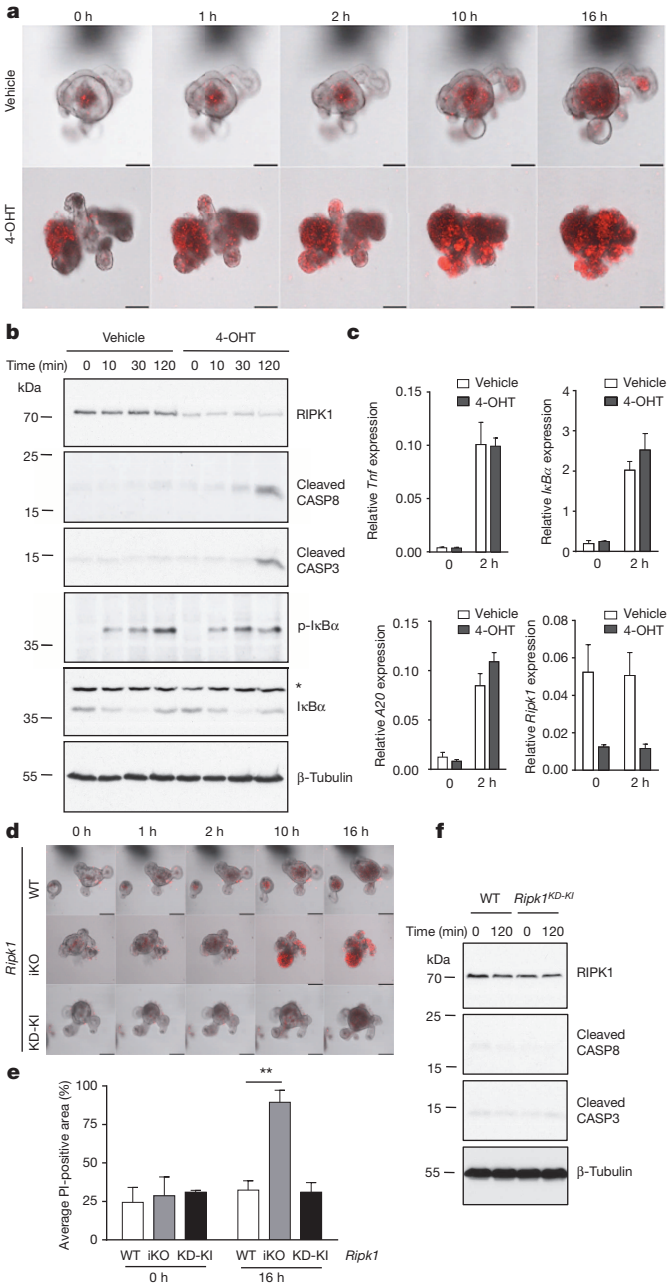

Figure 4 | $Ripk1^{IEC\text{-}KO}$ intestinal organoids are sensitized to TNF-induced apoptosis independently of NF-κB and kinase activity. Intestinal organoids were derived from $Ripk1^{iIEC\text{-}KO}$ mice; RIPK1 deletion was induced *in vitro* by 4-OHT treatment (200 nM) for 20−24 h after which organoids were treated with recombinant mouse TNF (mTNF). **a**, Time-lapse confocal microscopic imaging of propidium iodide (PI)-stained organoids. Scale bars, 100 μm. **b**, Western blot analysis of organoid cultures at different time points after mTNF administration. p-IκBα, phosphorylated IκBα. **c**, qPCR analysis of organoids stimulated with mTNF for 2 h ($n = 3$ biological replicates). Data represent mean ± s.e.m. A20, TNFα-induced protein 3. **d**, Intestinal organoids derived from $Ripk1^{fl/fl}$ (wild type, WT), $Ripk1^{iIEC\text{-}KO}$ (iKO) and $Ripk1^{KD\text{-}KI}$ mice were treated with mTNF as in **a**. **e**, Image analysis of the per cent of propidium-iodide-positive nuclei as in **d** ($n = 3$, biological triplicates). $^{**}P < 0.01$. Data represent mean ± s.e.m. WT, wild type; iKO, inducible knockout. **f**, Western blot analysis of organoid cultures after mTNF administration as in **d**.

necroptosis. Disease kinetics differ between the two studies and the pathology of our $Ripk1^{IEC\text{-}KO}$ mice is milder and consequently may be better protected by rescue experiments using antibiotics or genetic deletions such as $Tnfr1^{-/-}$ or $Myd88^{-/-}$. The reasons for these differences in severity of disease symptoms are not clear, but might be explained by

small variances in the genetic makeup of the mice strains used in different laboratory settings.

Online Content Methods, along with any additional Extended Data display items and Source Data, are available in the online version of the paper; references unique to these sections appear only in the online paper.

Received 16 February; accepted 23 July 2014.

1. Declercq, W., Vanden Berghe, T. & Vandenabeele, P. RIP kinases at the crossroads of cell death and survival. *Cell* **138,** 229–232 (2009).
2. Ofengeim, D. & Yuan, J. Regulation of RIP1 kinase signalling at the crossroads of inflammation and cell death. *Nature Rev. Mol. Cell Biol.* **14,** 727–736 (2013).
3. Kelliher, M. A. *et al.* The death domain kinase RIP mediates the TNF-induced NF-κB signal. *Immunity* **8,** 297–303 (1998).
4. Berger, S. B. *et al.* Cutting edge: RIP1 kinase activity is dispensable for normal development but is a key regulator of inflammation in SHARPIN-deficient mice. *J. Immunol.* **192,** 5476–5480 (2014).
5. Newton, K. *et al.* Activity of protein kinase RIPK3 determines whether cells die by necroptosis or apoptosis. *Science* **343,** 1357–1360 (2014).
6. Cho, Y. S. *et al.* Phosphorylation-driven assembly of the RIP1–RIP3 complex regulates programmed necrosis and virus-induced inflammation. *Cell* **137,** 1112–1123 (2009).
7. He, S. *et al.* Receptor interacting protein kinase-3 determines cellular necrotic response to TNF-α. *Cell* **137,** 1100–1111 (2009).
8. Zhang, D. W. *et al.* RIP3, an energy metabolism regulator that switches TNF-induced cell death from apoptosis to necrosis. *Science* **325,** 332–336 (2009).
9. Murphy, J. M. *et al.* The pseudokinase MLKL mediates necroptosis via a molecular switch mechanism. *Immunity* **39,** 443–453 (2013).
10. Sun, L. *et al.* Mixed lineage kinase domain-like protein mediates necrosis signaling downstream of RIP3 kinase. *Cell* **148,** 213–227 (2012).
11. Tenev, T. *et al.* The ripoptosome, a signaling platform that assembles in response to genotoxic stress and loss of IAPs. *Mol. Cell* **43,** 432–448 (2011).
12. Feoktistova, M. *et al.* cIAPs block ripoptosome formation, a RIP1/caspase-8 containing intracellular cell death complex differentially regulated by cFLIP isoforms. *Mol. Cell* **43,** 449–463 (2011).
13. Dondelinger, Y. *et al.* RIPK3 contributes to TNFR1-mediated RIPK1 kinase-dependent apoptosis in conditions of cIAP1/2 depletion or TAK1 kinase inhibition. *Cell Death Differ.* **20,** 1381–1392 (2013).
14. Bertrand, M. J. *et al.* cIAP1 and cIAP2 facilitate cancer cell survival by functioning as E3 ligases that promote RIP1 ubiquitination. *Mol. Cell* **30,** 689–700 (2008).
15. Ea, C. K., Deng, L., Xia, Z. P., Pineda, G. & Chen, Z. J. Activation of IKK by TNFα requires site-specific ubiquitination of RIP1 and polyubiquitin binding by NEMO. *Mol. Cell* **22,** 245–257 (2006).
16. O'Donnell, M. A., Legarda-Addison, D., Skountzos, P., Yeh, W. C. & Ting, A. T. Ubiquitination of RIP1 regulates an NF-κB-independent cell-death switch in TNF signaling. *Curr. Biol.* **17,** 418–424 (2007).
17. Kajino-Sakamoto, R. *et al.* TGF-β-activated kinase 1 signaling maintains intestinal integrity by preventing accumulation of reactive oxygen species in the intestinal epithelium. *J. Immunol.* **185,** 4729–4737 (2010).
18. Nenci, A. *et al.* Epithelial NEMO links innate immunity to chronic intestinal inflammation. *Nature* **446,** 557–561 (2007).
19. Günther, C. *et al.* Caspase-8 regulates TNF-α-induced epithelial necroptosis and terminal ileitis. *Nature* **477,** 335–339 (2011).
20. Welz, P. S. *et al.* FADD prevents RIP3-mediated epithelial cell necrosis and chronic intestinal inflammation. *Nature* **477,** 330–334 (2011).
21. Vince, J. E. *et al.* Inhibitor of apoptosis proteins limit RIP3 kinase-dependent interleukin-1 activation. *Immunity* **36,** 215–227 (2012).
22. Sato, T. *et al.* Single Lgr5 stem cells build crypt-villus structures *in vitro* without a mesenchymal niche. *Nature* **459,** 262–265 (2009).
23. Gentle, I. E. *et al.* In TNF-stimulated cells, RIPK1 promotes cell survival by stabilizing TRAF2 and cIAP1, which limits induction of non-canonical NF-κB and activation of caspase-8. *J. Biol. Chem.* **286,** 13282–13291 (2011).
24. Vanlangenakker, N. *et al.* cIAP1 and TAK1 protect cells from TNF-induced necrosis by preventing RIP1/RIP3-dependent reactive oxygen species production. *Cell Death Differ.* **18,** 656–665 (2011).
25. Oberst, A. *et al.* Catalytic activity of the caspase-8–$FLIP_L$ complex inhibits RIPK3-dependent necrosis. *Nature* **471,** 363–367 (2011).
26. Kaiser, W. J. *et al.* RIP3 mediates the embryonic lethality of caspase-8-deficient mice. *Nature* **471,** 368–372 (2011).
27. Moujalled, D. M. *et al.* In mouse embryonic fibroblasts, neither caspase-8 nor cellular FLICE-inhibitory protein (FLIP) is necessary for TNF to activate NF-κB, but caspase-8 is required for TNF to cause cell death, and induction of FLIP by NF-κB is required to prevent it. *Cell Death Differ.* **19,** 808–815 (2012).
28. Dillon, C. P. *et al.* RIPK1 blocks early postnatal lethality mediated by caspase-8 and RIPK3. *Cell* **157,** 1189–1202 (2014).
29. Rickard, J. A. *et al.* RIPK1 regulates RIPK3-MLKL-driven systemic inflammation and emergency hematopoiesis. *Cell* **157,** 1175–1188 (2014).
30. Kaiser, W. J. *et al.* RIP1 suppresses innate immune necrotic as well as apoptotic cell death during mammalian parturition. *Proc. Natl Acad. Sci. USA* **111,** 7753–7758 (2014).
31. Dannoppel, M. *et al.* RIPK1 maintains epithelial homeostasis by inhibiting apoptosis and necroptosis. *Nature* http://dx.doi.org/10.1038/nature13608 (this issue).

Supplementary Information is available in the online version of the paper.

Acknowledgements We thank the Transgenic Mice Core Facility (IRC, VIB-UGent, Ghent) for their assistance. Villin-Cre, villin-Cre-ERT2 and RIPK3 knockout mice were provided by D. Gumucio (University of Michigan), S. Robine (Paris, France) and K. Newton and V. Dixit (Genentech), respectively. We thank A. Bredan for editing the manuscript, and P. De Bleser and M. Vuylsteke for statistical analysis. P.V. is senior full professor at Ghent University and holder of a Methusalem grant. L.V. is holder of a fellowship from Research Foundation Flanders (FWO). W.D. and G.V.L. have research professor positions at Ghent University. M.B. has a tenure track position in the Multidisciplinary Research Program of Ghent University (GROUP-ID). N.T. and V.G. are paid by the Methusalem grant, S.L. by a VIB grant and S.K. by a grant from the FWO. G.V.L. was supported by an FWO Odysseus Grant and by research grants from FWO, Foundation against Cancer and the Queen Elisabeth Medical foundation. Research in P.V.'s group is supported by Belgian grants (Interuniversity Attraction Poles, IAP 7/32), Flemish grants (Research Foundation Flanders, FWO G.0875.11, FWO G.0973.11, FWO G.0A45.12N, FWO G.0787.13N, G.0544.11N, G0C3114N and Methusalem grant BOF09/01M00709), Ghent University grants (MRP, GROUP-ID consortium), grant from the Foundation against Cancer (F94 and 2010-162) and grants from VIB. C.B. and C.G. received funding from the IZKF of the FAU Erlangen-Nürnberg and the DFG within the projects SPP1656, BE3686/2 and SFB796.

Author Contributions N.T., L.V., M.J.M.B., W.D., G.v.L. and P.V. designed the study. N.T., L.V., M.J.M.B., L.D., T.D., M.S., S.K., V.G., S.L., C.G. and B.G. performed the experiments. N.T., L.V., M.J.M.B., A.G., W.D., G.v.L. and P.V. analysed the data. N.T., M.J.M.B., W.D., G.v.L. and P.V. wrote the manuscript. S.B.B., C.B., J.B. and P.J.G. provided reagents and scientific insight.

Author Information Reprints and permissions information is available at www.nature.com/reprints. The authors declare no competing financial interests. Readers are welcome to comment on the online version of the paper. Correspondence and requests for materials should be addressed to P.V. (Peter.Vandenabeele@irc.vib-ugent.be).

METHODS

Mice. TNFR1-deficient[32] and MYD88-deficient mice[33] were described. Villin-Cre transgenic mice[34] were provided by D. Gumucio (University of Michigan) and villin-Cre-ERT2 mice[35] were a gift from S. Robine (Paris, France). RIPK3 knockout mice[36] were a gift from V. Dixit[36] (Genentech). RIPK1 kinase-dead knock-in mice were generated as described[4]. Conditional CASP8 knockout mice have been described[19]. Mice were housed in individually ventilated cages at the VIB Inflammation Research Center, in either specific pathogen-free or conventional animal facilities, as indicated. All experiments on mice were conducted according to institutional, national and European animal regulations. Animal protocols were approved by the ethics committee of Ghent University. Sample size estimation was done by using G power statistics. There was no randomization but stratification was used to achieve a similar sex ratio among experimental groups. No blinding was done.

Generation of IEC-specific RIPK1 knockout mice. To generate a conditional *Ripk1* allele, a targeting vector was designed to insert a floxed fragment containing *Ripk1* exon 3 into the *Ripk1* locus (Extended Data Fig. 1). A cassette containing a neomycin gene and flanked by Frt sites was inserted into the second intron of the *Ripk1* gene inside the region flanked by *loxP* sites. A 3.9-kilobase (kb) fragment was used as a 5′ homology region, a 0.7-kb fragment was placed between the two *loxP* sites, and a 3.8-kb fragment was used as a 3′ homology region. The targeting vector was NotI-linearized and electroporated into C57BL/6N-derived embryonic stem cells[37]. After positive and negative selection, surviving embryonic stem cell clones were expanded, and genomic DNA was extracted and analysed by Southern blot using 5′ and 3′ probes. Clones displaying proper integration (Extended Data Fig. 1b) were injected into 3.5-day-old blastocysts and transferred to the uteri of pseudo-pregnant foster mothers. Male chimaeras were mated with C57BL/6J females to obtain germline transmission of the *Ripk1* floxed allele (still containing the neomycin selection cassette) (designated as $Ripk1^{Nfl}$). The Frt-flanked neomycin cassette was removed by crossing $Ripk1^{Nfl}$ mice with a Flp-deleter strain[38] to generate a *Ripk1* floxed allele ($Ripk1^{fl}$). $Ripk1^{fl/fl}$ mice were crossed to villin-Cre[22] and *villin-cre-ERT2* transgenic mice[35] to generate a constitutive IEC-specific RIPK1 knockout ($Ripk1^{IEC\text{-}KO}$) or 4-hydroxytamoxifen (4-OHT) inducible RIPK1 knockout ($Ripk1^{iIEC\text{-}KO}$). For *in vivo* inducible *Ripk1* deletion, $Ripk1^{iIEC\text{-}KO}$ mice were injected intraperitoneally once a day for five consecutive days with 1 mg 4-OHT (Sigma-Aldrich), as previously described[39]. All experiments were performed on mice backcrossed into the C57BL/6 genetic background for at least ten generations.

Mouse embryonic fibroblasts. Heterozygous $Ripk1^{+/-}$ mice were generated by crossing chimaeras transmitting the $Ripk1^{Nfl}$ genotype with Cre-deleter mice[40]. MEF cells were isolated from $Ripk1^{+/+}$, $Ripk1^{+/-}$ and $Ripk1^{-/-}$ embryos on day 14.5 and cultured in Dulbecco's modified Eagle's medium supplemented with 10% fetal calf serum, gentamycin (0.1 mg ml^{-1}), glutamine (0.3 mg ml^{-1}), non-essential amino acids (0.1 mM), and 0.1% β-mercaptoethanol (Gibco).

Southern and western blot and PCR analysis. For screening of correctly targeted embryonic stem cells, Southern blot analysis was performed to check correct 5′ and 3′ integration using a 5′ probe and a 3′ probe. Genomic DNA for Southern blot analysis was prepared as follows: cells were lysed overnight at 55 °C in a humidified chamber in 500 µl of lysis buffer (10 mM Tris-HCl pH 7.5, 10 mM EDTA, 10 mM NaCl and 0.5% sarcosyl, augmented with 1 µg ml^{-1} proteinase K just before use). 500 µl of isopropanol was added, plates were shaken at room temperature for 1 h, and the DNA pellet was washed and resuspended in 100 µl TE buffer with shaking at 37 °C. Southern blot analysis was performed after digestion of 35 µl of genomic DNA with ScaI to differentiate between 10.3-kb and 4.0-kb fragments (5′ probe), or with PvuII to differentiate between 10.0-kb and 5.3-kb fragments (3′ probe), corresponding to wild-type and $Ripk1^{NFL}$ alleles, respectively. DNA was separated in 2% agarose gels and transferred to nitrocellulose. Hybridization was performed with a ^{32}P-labelled probe. Protein lysates were prepared from MEF cells, IECs and organoid samples. Proteins were separated by SDS–PAGE, transferred to nitrocellulose, and analysed by immunoblotting. RIPK1 was detected with mouse monoclonal anti-RIPK1 (61459; BD Biosciences). The antibodies used were p-IKKα/β (Ser176/180, Cell Signaling Technology), IKKβ (2684, Cell Signaling Technology), p-IkBα (9246, Cell Signaling Technology), IkBβ (sc-945, Santa Cruz), p-JNK (44382G, Invitrogen), JNK (sc-572, Santa Cruz), phospho-p38 (9211, Cell Signaling Technology), p38 (9212, Cell Signaling Technology), cleaved CASP3 (9661, Cell Signaling Technology), β-tubulin (Abcam), cleaved CASP8 (9429, Cell Signaling Technology), cIAP1 (ALX-803-335-C100, Enzo Life Sciences), cFLIP (AG-20B-0005 (Dave-2), Adipogen) and TRAF2 (sc-876 (C-20), Santa Cruz). Mice were genotyped by PCR using forward primer 5′-CCCAGGTAGGTGGCACTGTAAGGCAGTCTG-3′ and reverse primer 5′-GGCAAACACCTTTAATCCAAGCCTGGTC-3′ to generate a 287-base-pair PCR fragment for the wild-type allele and a 361-base-pair PCR fragment for the $Ripk1^{Nfl}$ allele.

Histology. Formalin-fixed tissue was embedded in paraffin and 4-µm sections were cut and stained with haematoxylin and eosin. For immunohistochemistry, sections were dewaxed, incubated in Dako antigen retrieval solution (DAKO) at boiling temperature for 20 min in a Pick cell cooking unit, and cooled down for 2.5 h. Endogenous peroxidase activity was blocked by immersing the slides in peroxidase-blocking buffer (40 mM citric acid, 121 mM disodium hydrogen phosphate, 30 mM sodium azide, 1.5% hydrogen peroxide) for 15 min at room temperature. Blocking buffer (1% bovine serum albumin in PBS) was added to the slides for 30 min at room temperature. Primary antibody against cleaved CASP3 (Cell Signaling Technology) was incubated overnight in bovine serum albumin in PBS. Slides were then incubated with secondary antibody (polymer-horseradish-peroxidase-labelled anti-mouse/rabbit, Envision) and peroxidase was detected by diaminobutyric acid substrate. Slides were counterstained with Mayer's haematoxylin and mounted in Pertex mounting medium. For lysozyme staining, sections were incubated with DyLight-488 conjugated goat anti-rabbit secondary antibodies (Fisher Bioblock Scientific), and cell nuclei were counterstained with DAPI (Invitrogen) in ProLong Gold anti-fade reagent (Life Technologies). Immunohistochemistry for RIPK3 was performed by using an antibody against mRIPK3 (ADI-905-242-100 Enzo Life Sciences). Apoptosis was analysed with an *in situ* cell death detection kit (TMR-red, Roche) after antigen retrieval. Fluorescence microscopy was performed using a TCS SP5 confocal microscope (Leica).

FITC–dextran intestinal permeability assay. Intestinal permeability was assessed by oral gavage of FITC–dextran (Sigma), a macromolecule that cannot be metabolized and is used as a permeability probe. Mice were administered 100 µl FITC–dextran (600 mg per kg body weight) by oral gavage 4 h before killing. Whole blood was obtained by cardiac puncture at the time of killing, and FITC–dextran levels in 100 µl of serum were measured by fluorometry (488 nm). Serial dilutions of FITC–dextran in PBS were used to generate a standard curve.

Endoscopic analysis. High-resolution mouse endoscopy was performed as previously described[41] with a 'Coloview' endoscopic system (Karl Storz). Mice were anaesthetized with 2−2.5% isoflurane in oxygen during endoscopy.

Depletion of commensal bacteria. Breeding couples and offspring were treated with 200 mg ciprofloxacin (Sigma-Aldrich), 1 g ampicillin (Sigma-Aldrich), 1 g metronidazole (Sigma-Aldrich), and 500 mg vancomycin (Labconsult) per litre of drinking water 2 weeks before the expected birth of offspring. Drinking water and bedding were refreshed every 2−3 days. After 3 weeks, the presence of colonic microflora was determined by culturing faecal samples in liquid cultures in both 'Brain Heart Infusion' and 'Thioglycollate' medium (Sigma), and one-quarter dilutions of the liquid culture were plated on McConkey agar. Samples from individual mice were used. No growth from antibiotic-treated mice in any of the media was observed.

Quantitative real-time PCR. Total RNA was isolated from MEFs and mucosa of the small intestine. Freshly isolated ileal segments 5-cm long were flushed with PBS to remove faecal content. One end of the intestine was ligated and the intestine was filled with RNA lysis buffer (Aurum Total RNA Mini kit, Bio-Rad Laboratories) and kept on ice for 5 min. RNA was purified using the Aurum Total RNA Mini kit (Bio-Rad Laboratories) and cDNA was synthesized by using the iScript cDNA synthesis kit (Bio-Rad Laboratories) according to the manufacturer's instructions. 10 ng of cDNA was used for quantitative PCR in a total volume of 10 µl with LightCycler 480 SYBR Green I Master Mix (Roche) on a LightCycler 480 (Roche). Real-time PCR reactions were performed in triplicates. The following mouse-specific primers were used: Lysozyme P forward, 5′- GCCAAGGTCTAACAATCGTTGTGAGTTG-3′; Lysozyme P reverse, 5′-CAGTCAGCCAGCTTGACACCACG-3′; Cryptidin 1 forward, 5′-TCAAGAGGCTGCAAAGGAAGAGAAC-3′; Cryptidin 1 reverse, 5′-TGGTCTCCATGTTCAGCGACAGC-3′; A20 forward, 5′-AAACCAATGGTGATGGAAACTG-3′; A20 reverse, 5′-GTTGTCCCATTCGTCATTCC-3′; TNF forward, 5′-ACCCTGGTATGAGCCCATATAC-3′; TNF reverse, 5′-ACACCCATTCCCTTCACAGAG-3′; IL6 forward, 5′-GAGGATACCACTCCCAACAGACC-3′; IL6 reverse, 5′-AAGTGCATCATCGTTGTTCATACA-3′; MCP1 forward, 5′-GCATCTGCCCTAAGGTCTTCA-3′; MCP1 reverse, 5′-TGCTTGAGGTGGTTGTGGAA-3′; IκBα forward, 5′-GTAACCTACCAAGGCTACTC-3′; IκBα reverse, 5′-GCCACTTTCCACTTATAATGTC-3′; RIPK1 forward, 5′-GGTCAAATTCAGAACAACCTGGA-3′; RIPK1 reverse, 5′-CACACTGCGATCATTCTCGT-3′.

Isolation of intestinal crypts and 3D organoid culture. Intestinal organoids were derived from small intestine as previously described[42]. Briefly, a 5-cm piece of duodenum/jejunum was dissected and washed in PBS. The intestine was opened longitudinally, villi were scraped away, and the tissue was chopped into pieces of 2−3 mm. After thorough washing in PBS, the pieces were incubated in 2 mM EDTA/PBS for 30 min at 4 °C on a rocking platform. The mixture was passed through a 70-µm cell strainer, and crypt fractions were isolated and purified by successive centrifugation steps. One millilitre of Matrigel (BD Biosciences) was added to a pellet of 100−1000 crypts, and 50-µl drops of crypt-containing Matrigel were added to pre-warmed wells in a 24-well plate. After polymerization, 500 µl complete growth medium containing EGF (Peprotech), R-Spondin1 (R&D) and Noggin (Peprotech)[22] was added and refreshed every 2 days. For RIPK1 deletion, organoids were treated for 20−24 h with 200 nM 4-OHT diluted in organoid growth medium. Organoids

were stimulated with recombinant mouse TNF produced in *Escherichia coli* at the VIB Protein Service Facility (specific activity 3.33×10^8 IU mg^{-1}) (10 ng ml^{-1} or 25 ng ml^{-1}), lipopolysaccharide (100 μg ml^{-1}, Sigma) or lipotechoic acid (100 μg ml^{-1}, Sigma) after removing 4-OHT.

Live cell imaging of intestinal organoids. Images were acquired using a Leica TCS SP5 confocal system, using a 10X HC PL Apo CS 0.4 dry objective. The system was maintained at 37 °C in 5% CO_2. Images were acquired in a format of 1024 × 1024, with a line average of 2, scan speed of 700 Hz, and pinhole of 2 airy units. Excitation for both propidium iodide and brightfield was done with the 543 laser line at 6%, with a detection band of 555−699 nm. DAPI was imaged with a 405 diode laser at 11% and a detection band of 409−488 nm. Images were acquired every 15 min for at least 16 h. Image reconstruction was performed on ImageJ software (http://rsb.info.nih.gov/ij/).

Image acquisition and analysis of organoid cell death. Intestinal organoids derived from mice of different genotypes were suspended in Matrigel and plated in black imaging 96-well plates (BD Falcon Imaging Plates Cat No 353219). RIPK1$^{iIEC\text{-}KO}$ organoids were treated with 200 nM 4-OHT 16−24 h before adding stimuli. Organoid images were acquired using BDPathway 855 high content imaging instrument, using a ×4 objective. The complete well was imaged using a 4 × 4 montage. Each image frame of the montage was automatically focused by the 'image autofocus' module. Image analysis was performed using Attovision software. Out-of-focus organoids (due to Matrigel embedding at different focal planes) were excluded from analysis. Hoechst- and propidium-iodide-positive regions of interest were identified in a two-step analysis. For each of the regions of interest identified by Hoechst segmentation, the percentage of propidium-iodide-positive area (subobject) was reported. Depending on the organoid culture, 30−100 organoids were analysed per well.

Statistical analysis. All experiments were repeated at least twice, with similar results. Data represent biological replicates. Appropriate statistical tests were used for every type of analysis. Data meet the assumptions of the statistical tests described for each figure. Log_2 conversion was used where appropriate. Results are expressed as the mean ± s.e.m. Differences between experimental groups were assessed for significance using a two-tailed unpaired Student *t*-test, or one-way ANOVA with Bonferroni's multiple comparison post-hoc test using GraphPad Prism. Data involving two variables were analysed by two-way ANOVA using GraphPad Prism or by restricted maximum likelihood variance components analysis. Birth and survival ratios were analysed by Fisher's exact test, Pearson's Chi-squared test and general linear mixed regression model of the form: y = constant + genotype × treatment + breeding pair + breeding pair litter + error. The model was fitted to the log-transformed binomial data, represented by y, recording the number of weaned mice out of those born. The interaction between the genotype and the antibiotic treatment was assessed by an analysis of deviance, as implemented in the generalized linear mixed model framework in Genstat Version 16. Survival data were analysed by log-rank (Mantel–Cox) tests.

32. Rothe, J. *et al.* Mice lacking the tumour necrosis factor receptor 1 are resistant to TNF-mediated toxicity but highly susceptible to infection by *Listeria* monocytogenes. *Nature* **364,** 798–802 (1993).
33. Adachi, O. *et al.* Targeted disruption of the *MYD88* gene results in loss of IL-1- and IL-18-mediated function. *Immunity* **9,** 143–150 (1998).
34. Madison, B. B. *et al.* Cis elements of the villin gene control expression in restricted domains of the vertical (crypt) and horizontal (duodenum, cecum) axes of the intestine. *J. Biol. Chem.* **277,** 33275–33283 (2002).
35. El Marjou, F. *et al.* Tissue-specific and inducible Cre-mediated recombination in the gut epithelium. *Genesis* **39,** 186–193 (2004).
36. Newton, K., Sun, X. & Dixit, V. M. Kinase RIP3 is dispensable for normal NF-κBs, signaling by the B-cell and T-cell receptors, tumor necrosis factor receptor 1, and toll-like receptors 2 and 4. *Mol. Cell. Biol.* **24,** 1464–1469 (2004).
37. Schoonjans, L. *et al.* Improved generation of germline-competent embryonic stem cell lines from inbred mouse strains. *Stem Cells* **21,** 90–97 (2003).
38. Rodríguez, C. I. *et al.* High-efficiency deleter mice show that FLPe is an alternative to Cre-loxP. *Nature Genet.* **25,** 139–140 (2000).
39. Metzger, D. & Chambon, P. Site- and time-specific gene targeting in the mouse. *Methods* **24,** 71–80 (2001).
40. Betz, U. A., Vosshenrich, C. A., Rajewsky, K. & Muller, W. Bypass of lethality with mosaic mice generated by Cre–loxP-mediated recombination. *Curr. Biol.* **6,** 1307–1316 (1996).
41. Becker, C., Fantini, M. C. & Neurath, M. F. High resolution colonoscopy in live mice. *Nature Protocols* **1,** 2900–2904 (2007).
42. Sato, T. & Clevers, H. Primary mouse small intestinal epithelial cell cultures. *Methods Mol. Biol.* **945,** 319–328 (2013).

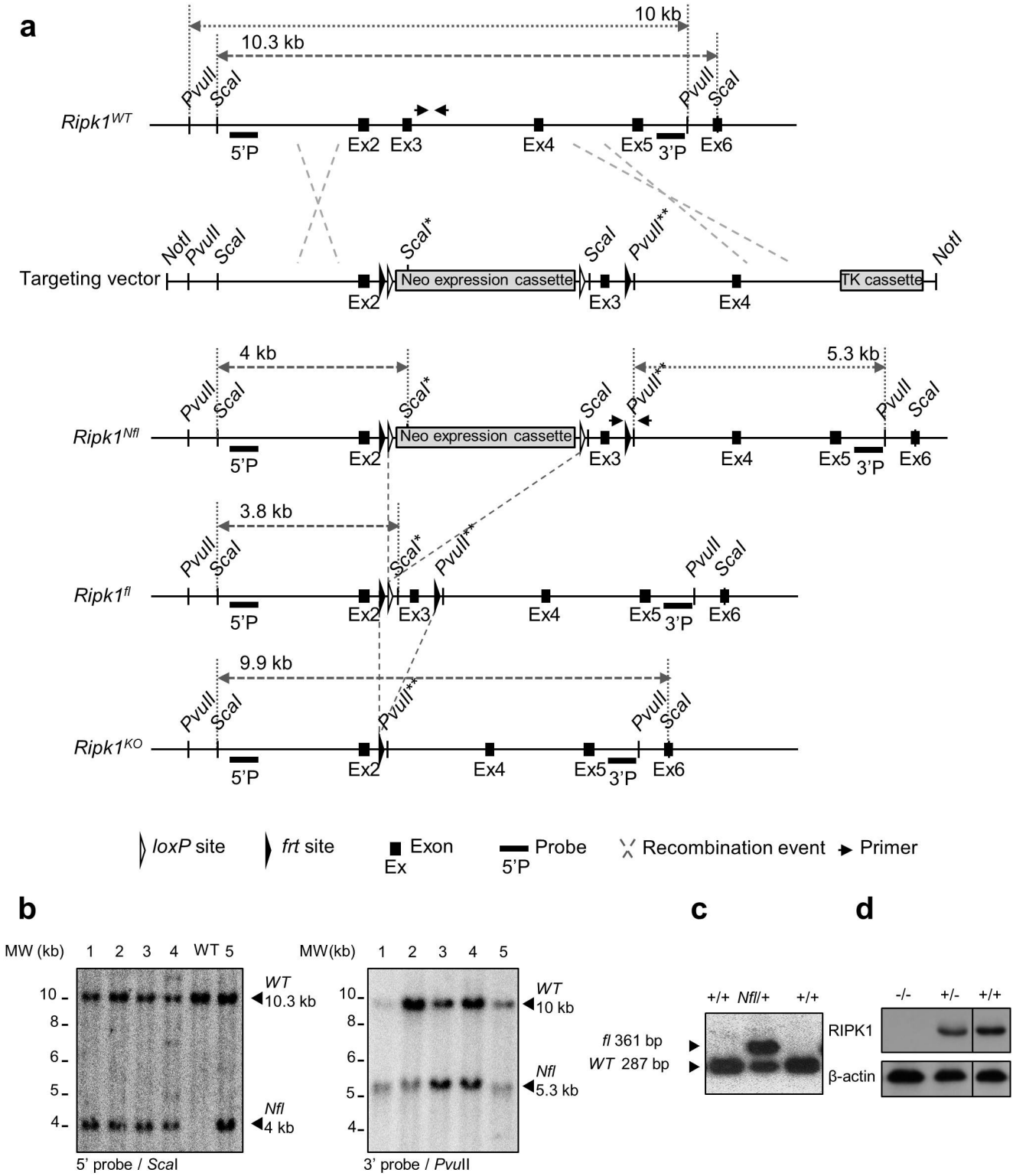

Extended Data Figure 1 | Generation of conditional *Ripk1*$^{-/-}$ mice using Cre–*loxP* technology. **a**, Schematic representation of the targeting vector along with wild-type and mutant loci. Double homologous recombination between the wild-type *Ripk1* allele and the targeting vector leads to entry of the neomycin positive selection marker and of extra ScaI (*) and PvuII (**) restriction sites in the *Ripk1* allele and exclusion of the thymidine kinase (TK) negative selection marker, generating the *Ripk1*^{Nfl} allele. Southern blot analysis reveals a 4.0-kb DNA fragment instead of a 10.3-kb fragment with the 5′ probe and a 5.3-kb instead of a 10.0-kb fragment with the 3′ probe for the *Ripk1*^{Nfl} allele compared to the wild-type *Ripk1*. The Frt-flanked neomycin cassette was removed by crossing *Ripk1*^{Nfl} mice with a Flp-deleter strain to generate a *Ripk1* floxed allele (*Ripk1*^{fl}). To ablate RIPK1, *Ripk1*$^{fl/fl}$ mice were crossed with Cre-deleter transgenic mice to induce germline recombination of the *loxP* sequences or with cell-type-specific Cre transgenic lines to induce tissue-specific recombination. The *loxP* interstitial exon 3 is looped out, disabling *Ripk1* transcription. **b**, Southern blot analysis of five positive embryonic stem cell clones using a 5′ probe and a 3′ probe. MW, molecular weight; WT, wild type; Rec, recombinant. **c**. *Ripk1*$^{+/+}$ and *Ripk1*$^{Nfl/+}$ genotypes were distinguished by PCR using the primers indicated by arrows in **a**. **d**, MEF cells were prepared from *Ripk1*$^{+/+}$, *Ripk1*$^{+/-}$ and *Ripk1*$^{-/-}$ embryos on embryonic day 14.5, and RIPK1 protein levels were analysed in lysates by western blot. β-Actin protein levels were used as a loading control.

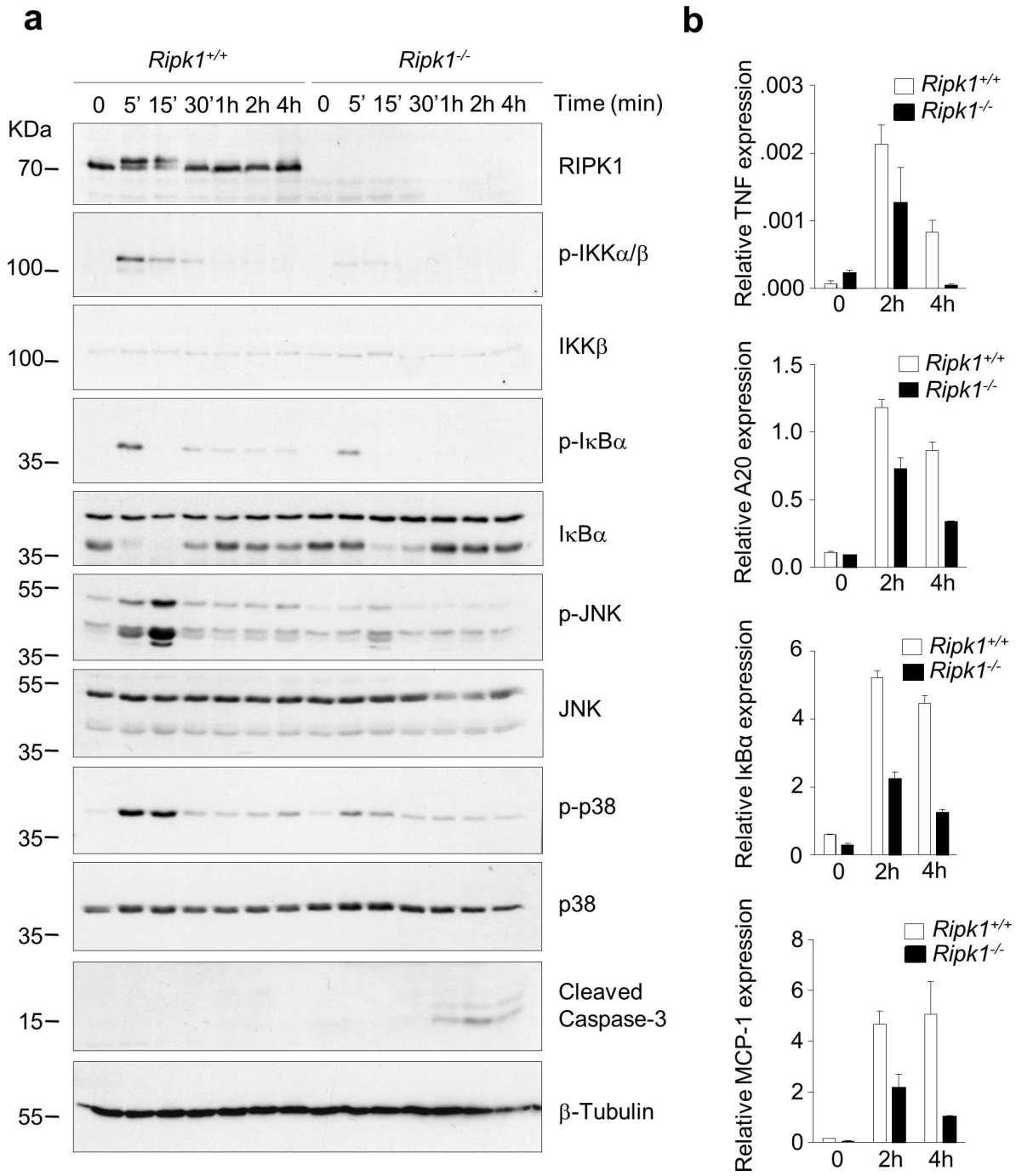

Extended Data Figure 2 | RIPK1 deficiency in MEFs results in defective MAPK and NF-κB activation associated with apoptosis induction upon TNF stimulation. *Ripk1*$^{-/-}$ MEFs and control *Ripk1*$^{+/+}$ MEFs were stimulated with 10 ng ml^{-1} of mTNF. **a**, Western blot analysis of NF-κB and MAPK activation in lysates sampled at different time points. **b**, RNA was analysed by qPCR for TNF, A20, IκBα and MCP1 expression ($n = 3$). Data are represented by mean ± s.e.m.

a

Ripk1$^{fl/fl}$ x *Ripk1*$^{fl/+}$*villin-cre*^{Tg}

	Born		Weaned	
	Expected	Observed	Expected	Observed
Ripk1$^{fl/fl}$*cre*^{Tg}	25 % (19,25)	15,6 % (12)	25 % (11.75)	4,3 % (2)
Ripk1$^{fl/fl}$	25 % (19,25)	29,9 % (23)	25 % (11.75)	36,2 % (17)
Ripk1$^{fl/+}$*cre*^{Tg}	25 % (19,25)	27,3 % (21)	25 % (11.75)	34,0 % (16)
Ripk1$^{fl/+}$	25 % (19,25)	20,8 % (16)	25 % (11.75)	25,5 % (12)
Ripk1$^{fl/-}$*cre*^{Tg}	0	6,5 % (5)	0	0
Total (Observed)	100 % (77)	100 % (77)	100 % (47)	100% (47)
P-value:	0.108		0.033*	

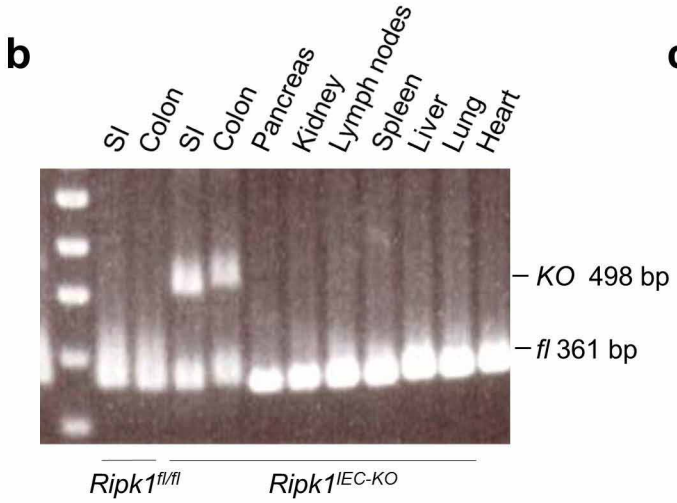

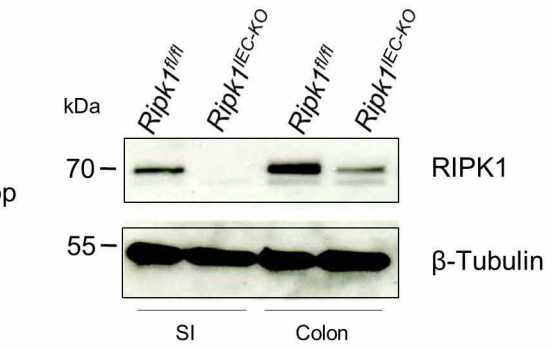

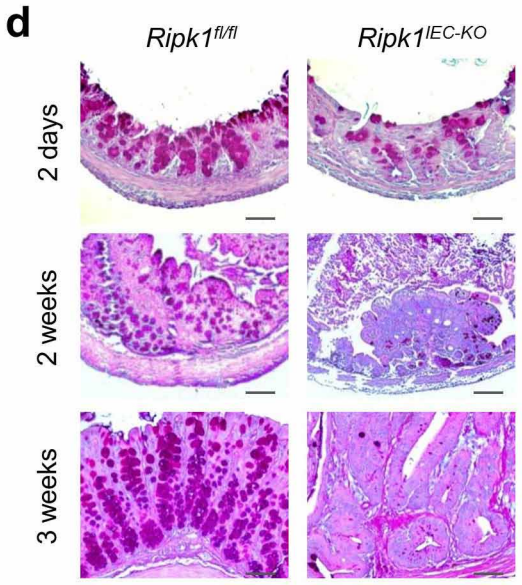

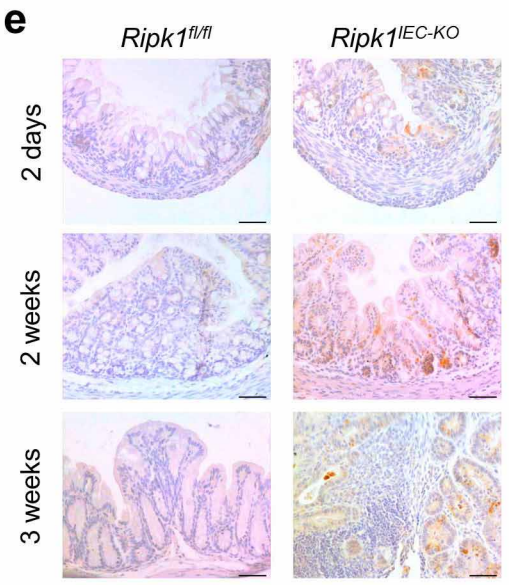

Extended Data Figure 3 | Characterization of *Ripk1*$^{IEC-KO}$ mice. **a**, Birth and survival rates of all genotypes of offspring from selected breeding couples (*Ripk1*$^{fl/fl}$ × *Ripk1*$^{fl/+}$ *villin-cre*^{Tg}). *$P < 0.05$ by Fischer's exact test. **b**, Genomic PCR analysis of *Ripk1* alleles on DNA extracted from various tissues of *Ripk1*$^{IEC-KO}$ mice and control *Ripk1*$^{fl/fl}$ mice. **c**, Western blot detection of RIPK1 protein in small intestine and colon tissue of *Ripk1*$^{IEC-KO}$ and control *Ripk1*$^{fl/fl}$ mice. KO, knockout; bp, base pairs. **d**, PAS/AB staining of colons of *Ripk1*$^{IEC-KO}$ and *Ripk1*$^{fl/fl}$ mice (the same sample set as in Fig. 1c). **e**, Immunohistochemistry of activated CASP3 in the same sample set as in **d**.

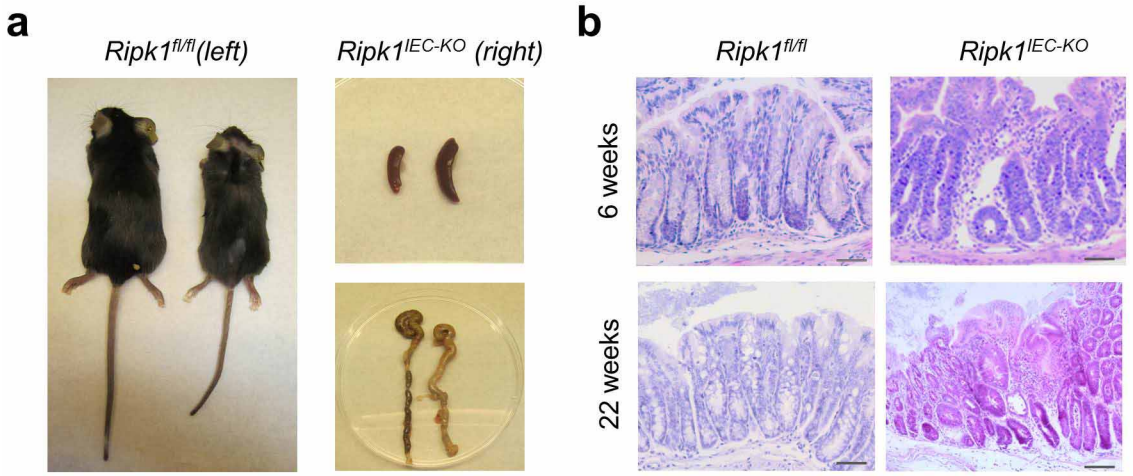

Extended Data Figure 4 | Characterization of older *Ripk1*$^{IEC\text{-}KO}$ mice. **a**, Macroscopic images showing 22-week-old *Ripk1*$^{fl/fl}$ and *Ripk1*$^{IEC\text{-}KO}$ mice, and corresponding splenomegaly and colon shortening in *Ripk1*$^{IEC\text{-}KO}$ mice. **b**, Haematoxylin and eosin staining of *Ripk1*$^{fl/fl}$ ($n = 3$) and *Ripk1*$^{IEC\text{-}KO}$ ($n = 3$) mice at the ages of 6 weeks and 22 weeks. A representative image is shown.

a

Ripk1$^{fl/fl}$ x *Ripk1*$^{fl/+}$ *villin-cre*^{Tg} with ABX

	Born		Weaned	
	Expected	Observed	Expected	Observed
Ripk1$^{fl/fl}$ *cre*^{Tg}	25 % (16)	28,1 % (18)	25 % (14)	26,8 % (15)
Ripk1$^{fl/fl}$	25 % (16)	18,9 % (12)	25 % (14)	16,1 % (9)
Ripk1$^{fl/+}$ *cre*^{Tg}	25 % (16)	28,1 % (18)	25 % (14)	30,4 % (17)
Ripk1$^{fl/+}$	25 % (16)	18,9 % (12)	25 % (14)	21,4 % (12)
Ripk1$^{fl/-}$ *cre*^{Tg}	0	6,3% (4)	0	5,4 % (3)
Total (Observed)	100 % (64)	100 % (64)	100 % (56)	100 % (56)
P-value:	0.280		0.390	

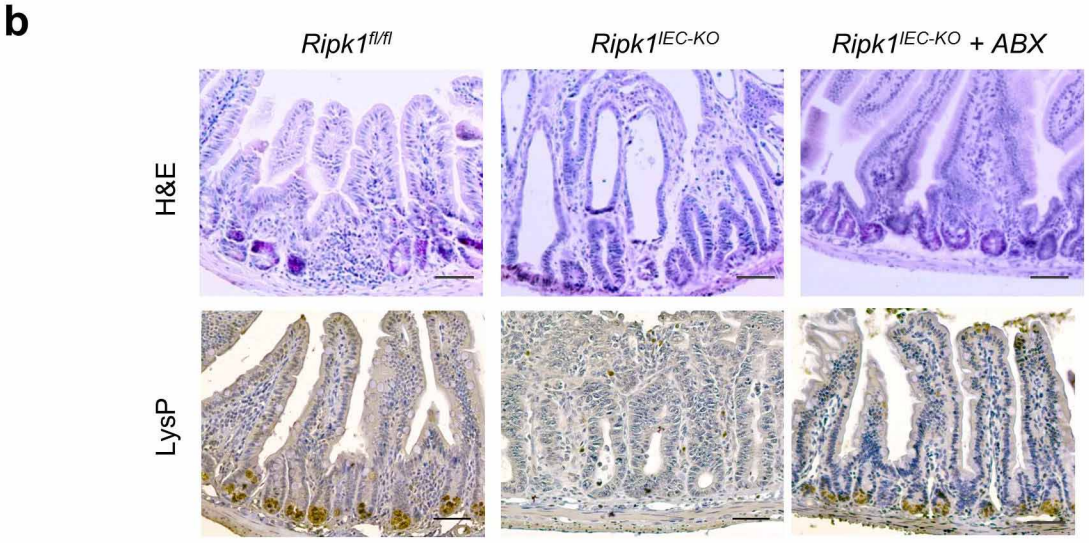

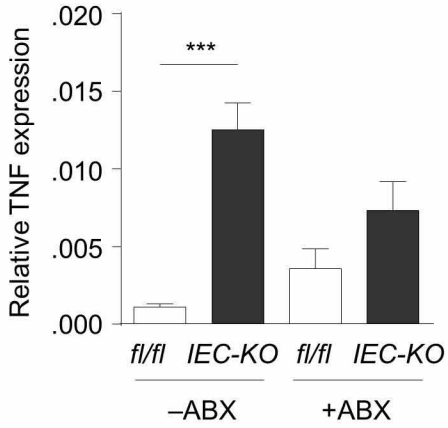

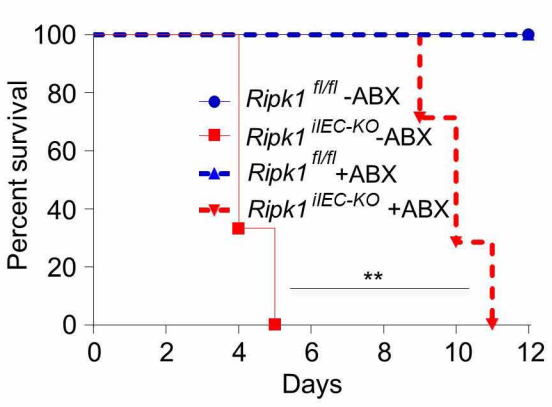

Extended Data Figure 5 | Rescue of the inflammatory phenotype of *Ripk1*$^{IEC-KO}$ mice by antibiotic treatment. **a**, Birth and survival rates (at weaning age) of all genotypes either treated or untreated with broad-spectrum antibiotics (ABX). The interaction between the genotype and the antibiotic treatment was assessed by analysis of deviance. **b**, Histopathological analysis by haematoxylin and eosin and immunohistochemical staining of Lysozyme P (LysP, Paneth cells) in small intestine samples from mice with or without antibiotic treatment: *Ripk1*$^{fl/fl}$ mice ($n = 5$), *Ripk1*$^{IEC-KO}$ mice without antibiotics ($n = 5$) and *Ripk1*$^{IEC-KO}$ mice with antibiotics ($n = 7$). **c**, TNF level detected by qPCR of RNA isolated from small intestine of antiobiotic-treated and non-treated *Ripk1*$^{fl/fl}$ and *Ripk1*$^{IEC-KO}$ mice (all $n = 5$). ***$P = 0.0001$ by two-tailed, two-way ANOVA. Data represent mean ± s.e.m. WT, wild type; KO, knockout. **d**, Antibiotic-treated *Ripk1*$^{fl/fl}$ ($n = 3$) and *Ripk1*$^{iIEC-KO}$ ($n = 7$), and non-treated *Ripk1*$^{fl/fl}$ ($n = 3$) and *Ripk1*$^{iIEC-KO}$ ($n = 5$) mice were subjected to RIPK1 deletion by daily treatment with 1 mg 4-OHT, and survival rate was monitored. ***$P = 0.0007$.

a *Ripk1$^{fl/fl}$ Myd88$^{-/-}$* x *Ripk1$^{fl/+}$ villin-cre^{Tg} Myd88$^{-/-}$*

	Born		Weaned	
	Expected	Observed	Expected	Observed
Ripk1$^{fl/fl}$ cre^{Tg} Myd88$^{-/-}$	25 % (5,5)	20,0 % (5)	25 % (5,5)	20,0 % (5)
Ripk1$^{fl/fl}$ Myd88$^{-/-}$	25 % (5,5)	24,0 % (6)	25 % (5,5)	24,0 % (6)
Ripk1$^{fl/+}$ cre^{Tg} Myd88$^{-/-}$	25 % (5,5)	24,0 % (6)	25 % (5,5)	24,0 % (6)
Ripk1$^{fl/+}$ Myd88$^{-/-}$	25 % (5,5)	20,0 % (5)	25 % (5,5)	20,0 % (5)
Total (Observed)	100 % (22)	100 % (22)	100 % (22)	100% (22)
P-value:	0.9929		0.9929	

b *Ripk1$^{fl/fl}$ Tnfr1$^{-/-}$* x *Ripk1$^{fl/+}$ villin-cre^{Tg} Tnfr1$^{-/-}$*

	Born		Weaned	
	Expected	Observed	Expected	Observed
Ripk1$^{fl/fl}$ cre^{Tg} Tnfr1$^{-/-}$	25 % (11,75)	23,4 % (11)	25 % (11.25)	24,4% (11)
Ripk1$^{fl/fl}$ Tnfr1$^{-/-}$	25 % (11,75)	27,6 % (13)	25 % (11.25)	28,8 % (13)
Ripk1$^{fl/+}$ cre^{Tg}Tnfr1-/-	25 % (11,75)	25,5 % (12)	25 % (11.25)	24,4 % (11)
Ripk1$^{fl/+}$ Tnfr1$^{-/-}$	25 % (11,75)	23,4 % (11)	25 % (11.25)	22,2 % (10)
Total (Observed)	100 % (47)	100 % (47)	100 % (45)	100% (45)
P-value:	0,99		0.9769	

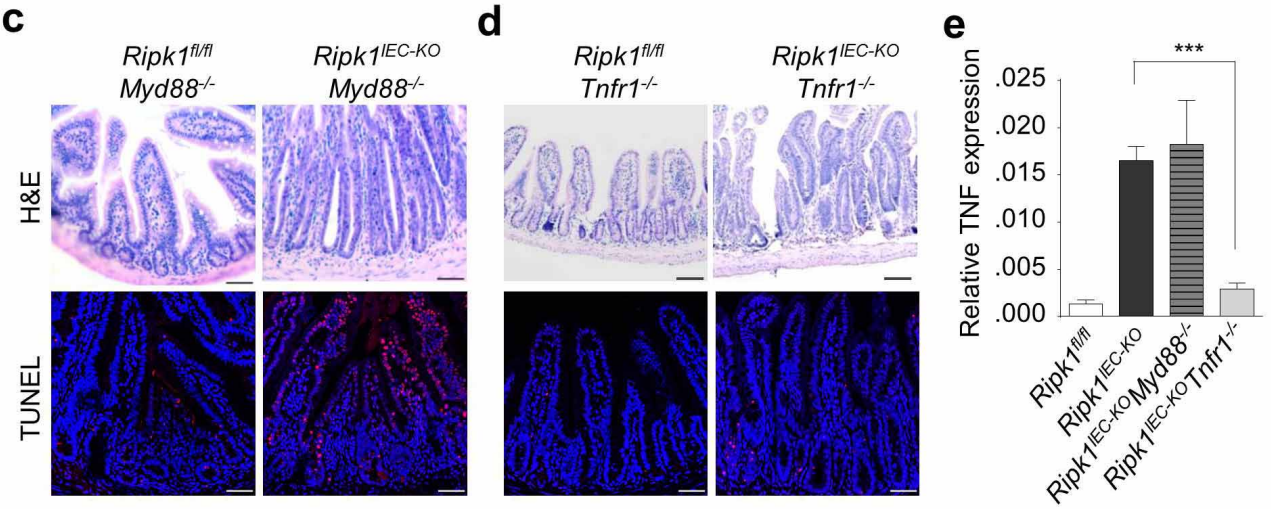

Extended Data Figure 6 | Rescue of the lethal phenotype of *Ripk1^{IEC-KO}* mice by MYD88 deficiency or TNFR1 deficiency. **a**, Birth and survival rates (at weaning age) of offspring of all genotypes from selected breeding couples (*Ripk1$^{fl/fl}$ Myd88$^{-/-}$* × *Ripk1$^{fl/+}$ villin-cre^{Tg} Myd88$^{-/-}$*); Pearson's χ^2 test. **b**, Birth and survival rates (at weaning age) of offspring of all genotypes from selected breeding couples (*Ripk1$^{fl/fl}$ Tnfr1$^{-/-}$* × *Ripk1$^{fl/+}$ villin-cre^{Tg} Tnfr1$^{-/-}$*); Pearson's χ^2 test. **c**, Haematoxylin and eosin staining and TUNEL assay of *Ripk1$^{fl/fl}$ Myd88$^{-/-}$* mouse and a littermate *Ripk1^{IEC-KO} Myd88$^{-/-}$* mouse small intestine. **d**, Haematoxylin and eosin staining and TUNEL assay of *Ripk1$^{fl/fl}$Tnfr1$^{-/-}$* mouse and a littermate *Ripk1^{IEC-KO}Tnfr1$^{-/-}$* mouse small intestine. **e**, TNF levels of small intestine lysate from *Ripk1$^{fl/fl}$* ($n = 5$), *Ripk1^{IEC-KO}*($n = 5$), *Ripk1^{IEC-KO} Myd88$^{-/-}$* ($n = 4$) and *Ripk1^{IEC-KO} Tnfr1$^{-/-}$* mouse ($n = 6$) determined by qPCR analysis.

a

Ripk1$^{fl/fl}$ *Casp8*$^{fl/fl}$ x *Ripk1*$^{fl/+}$ *Casp8*$^{fl/+}$ *villin-cre*^{Tg}

	Expected	Observed
Ripk1$^{fl/fl}$ *Casp8*$^{fl/fl}$ *cre*^{Tg}	12.5 % (7,4)	10,5 % (6)
Ripk1$^{fl/fl}$ *Casp8*$^{fl/fl}$	12.5 % (7,4)	14,0 % (8)
Ripk1$^{fl/fl}$ *Casp8*$^{fl/+}$ *cre*^{Tg}	12.5 % (7,4)	3,5 % (2)
Ripk1$^{fl/fl}$ *Casp8*$^{fl/+}$	12.5 % (7,4)	7,1 % (4)
Ripk1$^{fl/+}$ *Casp8*$^{fl/fl}$ *cre*^{Tg}	12.5 % (7,4)	19,3 % (11)
Ripk1$^{fl/+}$ *Casp8*$^{fl/fl}$	12.5 % (7,4)	17,5 % (10)
Ripk1$^{fl/+}$ *Casp8*$^{fl/+}$ *cre*^{Tg}	12.5 % (7,4)	17,5 %(10)
Ripk1$^{fl/+}$ *Casp8*$^{fl/+}$	12.5 % (7,4)	10,5% (6)
Total (Observed)	100 % (59)	100 % (57)

b

c

Ripk1$^{fl/fl}$ *Ripk3*$^{-/-}$ x *Ripk1*$^{fl/+}$ *Ripk3*$^{-/-}$ *villin-cre*^{Tg}

	Expected	Observed
Ripk1$^{fl/fl}$ *Ripk3*$^{-/-}$ *cre*^{Tg}	25 % (14,5)	10 % (5)**
Ripk1$^{fl/fl}$ *Ripk3*$^{-/-}$	25 % (14,5)	29 % (14)
Ripk1$^{fl/+}$ *Ripk3*$^{-/-}$ *cre*^{Tg}	25 % (14,5)	27 %(13)
Ripk1$^{fl/+}$ *Ripk3*$^{-/-}$	25 % (14,5)	35 % (17)
Total (Observed)	100 % (58)	100 % (49)

d

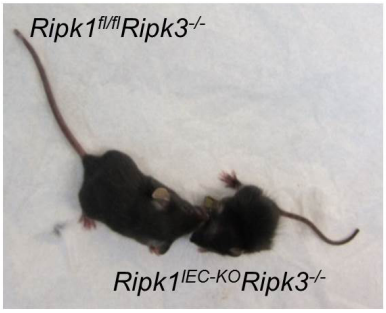

e

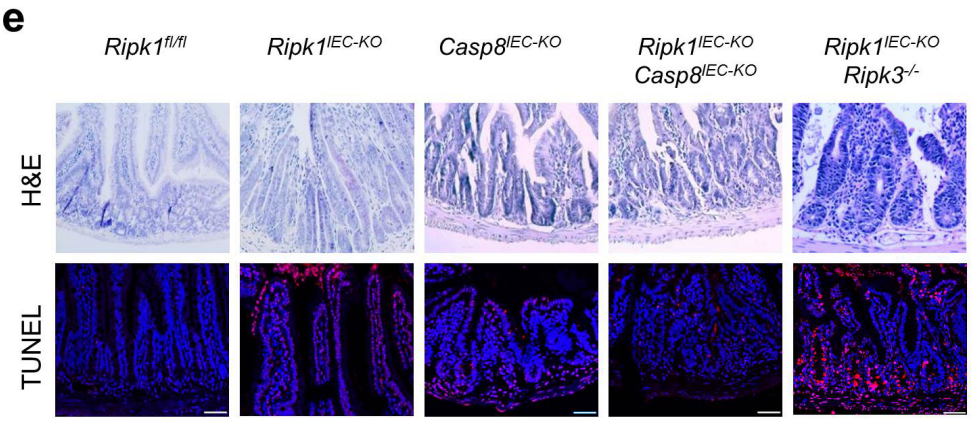

f

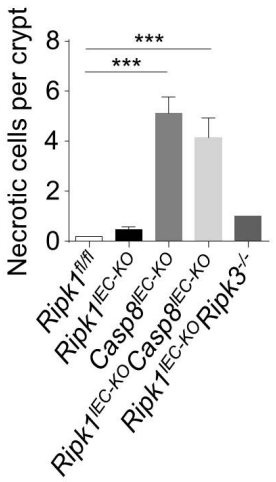

Extended Data Figure 7 | *Ripk1*$^{IEC\text{-}KO}$ phenotype involves CASP8 but not RIPK3. **a**, Survival rate of offspring of all genotypes from selected breeding couples (*Ripk1*$^{fl/fl}$ *Casp8*$^{fl/fl}$ × *Ripk1*$^{fl/+}$ *Casp8*$^{fl/+}$ *villin-cre*^{Tg}) at weaning. **b**, An image of a 26-week-old *Ripk1*$^{IEC\text{-}KO}$ *Casp8*$^{IEC\text{-}KO}$ mouse and a littermate *Ripk1*$^{fl/fl}$ *Casp8*$^{fl/fl}$ mouse showing no detectable difference. All *Ripk1*$^{IEC\text{-}KO}$ *Casp8*$^{IEC\text{-}KO}$ mice at different ages ($n = 6$) were indistinguishable from littermate *Ripk1*$^{fl/fl}$ *Casp8*$^{fl/fl}$ mice ($n = 8$). **c**, Survival rate of offspring all of genotypes from selected breeding couples (*Ripk1*$^{fl/fl}$*Ripk3*$^{-/-}$ × *Ripk1*$^{fl/+}$ *Ripk3*$^{-/-}$ *villin-cre*^{Tg}) at weaning showing significantly fewer *Ripk1*$^{fl/fl}$ *Ripk3*$^{-/-}$ mice surviving at weaning. **d**, An image of a 9-week-old *Ripk1*$^{IEC\text{-}KO}$ *Ripk3*$^{-/-}$ mouse and a littermate *Ripk1*$^{fl/fl}$ *Ripk3*$^{-/-}$ mouse. All *Ripk1*$^{IEC\text{-}KO}$*Ripk3*$^{-/-}$ mice at different ages ($n = 5$) were smaller than littermate *Ripk1*$^{fl/fl}$ *Casp8*$^{fl/fl}$ mice ($n = 14$). **e**, Haematoxylin and eosin staining and TUNEL assay of small intestine of *Ripk1*$^{IEC\text{-}KO}$, *Ripk1*$^{fl/+}$ *Casp8*$^{IEC\text{-}KO}$ (indicated as *Casp8*$^{IEC\text{-}KO}$), *Ripk1*$^{IEC\text{-}KO}$ *Casp8*$^{IEC\text{-}KO}$, *Ripk1*$^{IEC\text{-}KO}$ *Casp8*$^{IEC\text{-}KO}$ and *Ripk1*$^{IEC\text{-}KO}$ *Ripk3*$^{-/-}$ mice. **f**, The number of necrotic cells per crypt was counted based on haematoxylin and eosin staining.

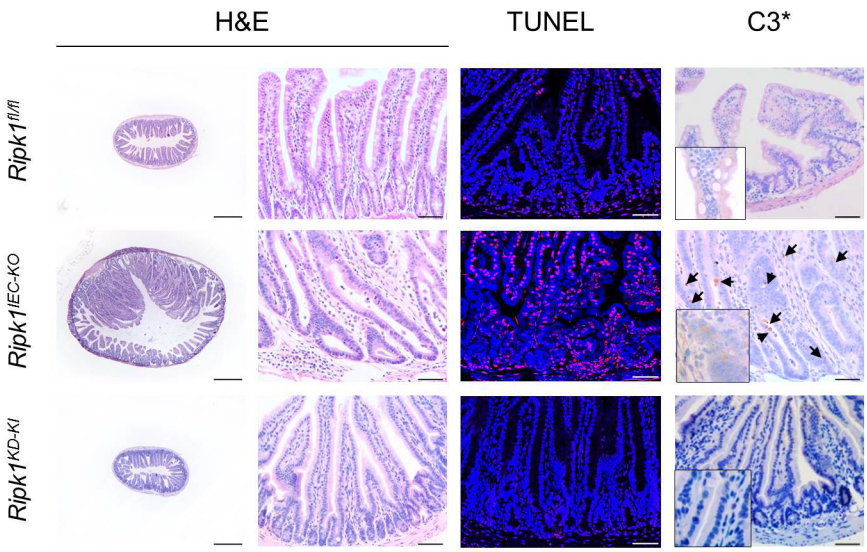

Extended Data Figure 8 | RIPK1 kinase activity is not required for intestinal homeostasis. Haematoxylin and eosin staining and TUNEL assay and immunohistochemical staining of active CASP3 (C3*) in small intestine samples from *Ripk1*$^{fl/fl}$ mice ($n = 5$), *Ripk1*$^{IEC\text{-}KO}$ mice ($n = 5$) and RIPK1-kinase-dead knock-in mice (*Ripk1*$^{KD\text{-}KI}$, $n = 5$) at the age of 6−14 weeks. The images of 12-week-old mice are shown. Scale bars, 50 μm; black arrows indicate active CASP3 positivity. A magnified view is inserted in the left corner of the immunohistochemistry images.

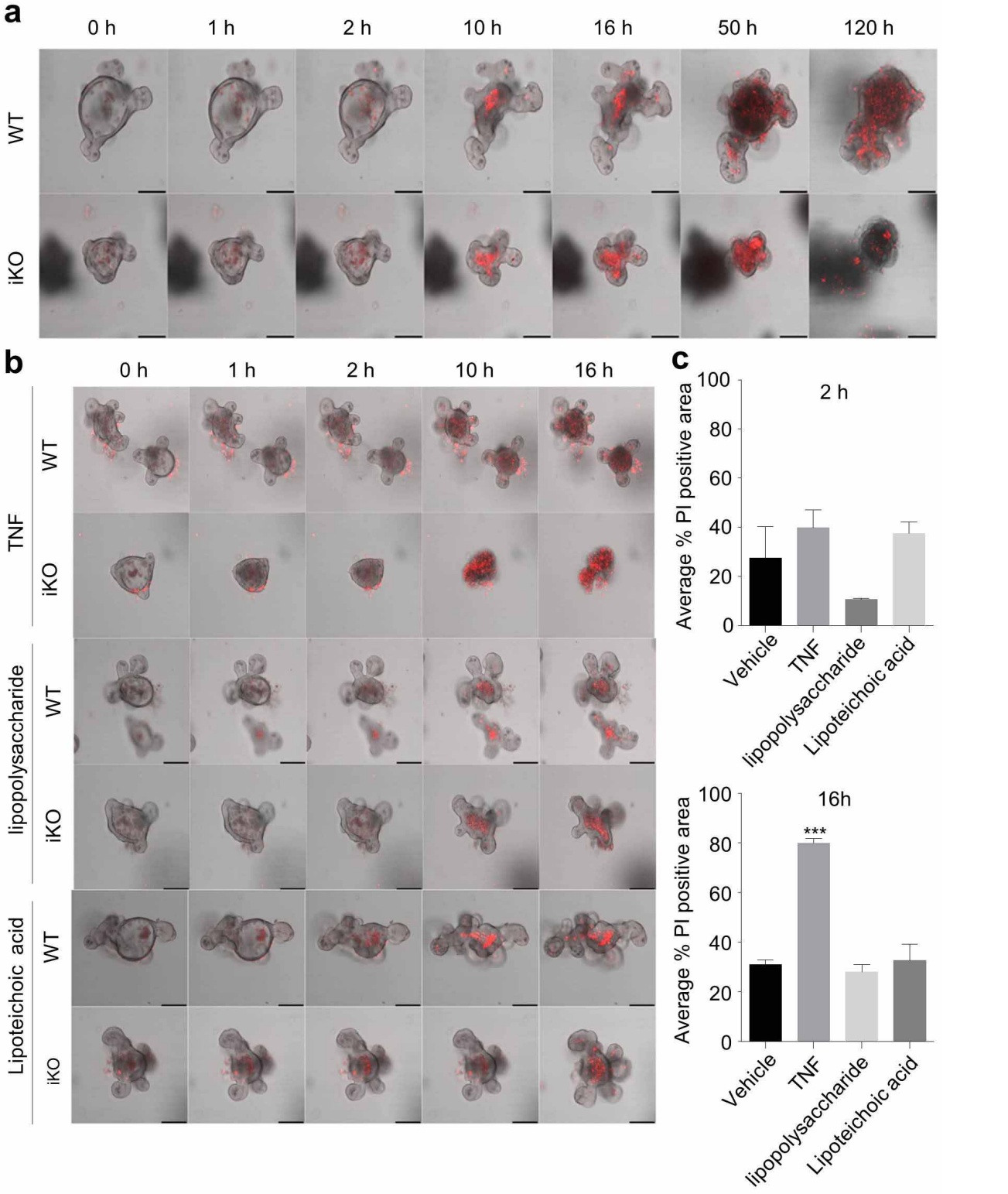

Extended Data Figure 9 | TNF-independent death of organoids and no direct cell death induction by TLR4 or TLR2 ligand. Intestinal organoids were derived from small intestine crypt cells isolated from wild-type (WT) and *Ripk1*$^{iIEC\text{-}KO}$ mice. RIPK1 deletion (iKO) was induced *in vitro* by 4-OHT treatment (200 nM) for 20−24 h. **a**, Organoids were observed for up to 4 days after removal of 4-OHT. **b**, Organoids were treated with 10 ng ml^{-1} mTNF, Gram-negative bacterial lipopolysaccharide (TLR4 ligand, 100 μg ml^{-1}), or Gram-positive bacterial lipoteichoic acid (TLR2 ligand, 100 μg ml^{-1}) after removal of 4-OHT. Time-lapse confocal microscopic imaging of propidium iodide (PI)-stained organoids ($n = 2$). Scale bar, 100 μm. **c**, Image analysis of the percentage of propidium-iodide-positive nuclei in an experiment resembling those in **b**.

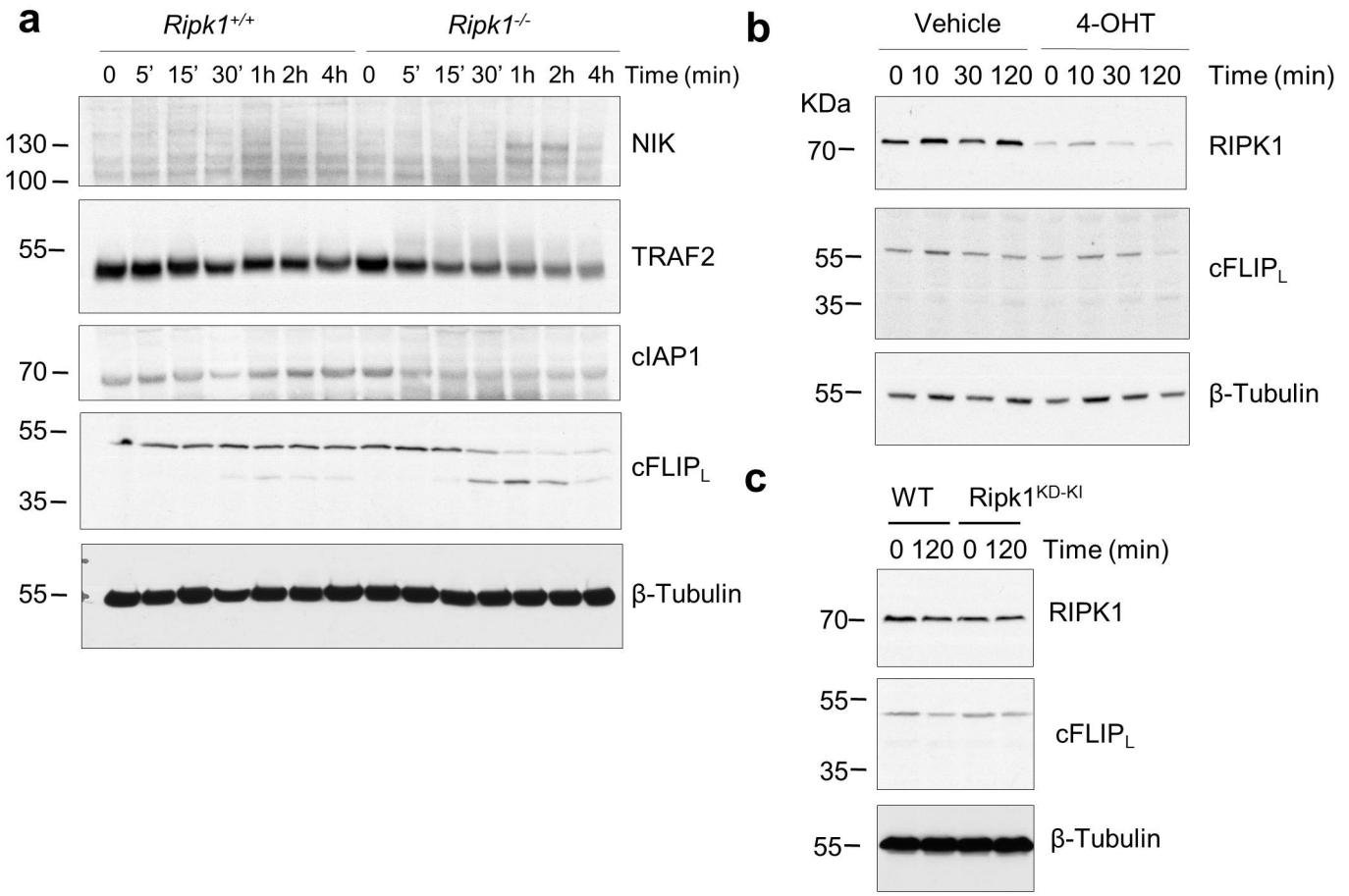

Extended Data Figure 10 | Degradation of cFLIP in TNF-treated *Ripk1*$^{-/-}$ MEFs and *Ripk1*$^{iIEC\text{-}KO}$ organoids. **a**, Protein lysates were prepared at designated times from *Ripk1*$^{-/-}$ MEFs treated with mTNF (10 ng ml^{-1}) and analysed by western blot for NF-κB-inducing kinase (NIK), TRAF2, cIAP1 and cFLIP. **b**, Protein lysates were prepared at designated times from *Ripk1*$^{iIEC\text{-}KO}$ organoids treated with 4-OHT (200 nM) for 20 h before stimulation with mTNF (10 ng ml^{-1}), and analysed by western blot for cIAP1. **c**, Protein lysates isolated from *Ripk1*$^{KD\text{-}KI}$ organoids were stimulated with mTNF (10 ng ml^{-1}) in an independent experiment and analysed for RIPK1 and cFLIP. WT, wild type.